Carbon Nanotube Vacuum Tube Diode RFID Tag

by

Michael Jung

A thesis submitted to the Graduate Faculty of
Auburn University
in partial fulfillment of the
requirements for the Degree of
Master of Science

Auburn, Alabama
December 12, 2015

Keywords: carbon nanotubes, vacuum tube diode,
Fowler-Norheim, field emission

Approved by

Hulya Kirkici, Chair, Professor of Electrical and Computer Engineering
Thomas Baginski, Professor of Electrical and Computer Engineering
Robert Dean, Associate Professor of Electrical and Computer Engineering

Abstract

Carbon Nanotubes (CNTs) have been studied for the past two decades and their research continues with new commercial and practical purposes. The structure of carbon and the many shapes it can form makes it an extremely versatile material. The study of very small structures of carbon poses difficulties in accurate description; hence many specialized ways have become standard to measure CNT properties. There are also many different ways of growing CNTs, which can lead to better performance, characteristics and fewer impurities. In this thesis, I study the field emission properties of CNTs and constructed a "vacuum-tube-diode" using CNTs. Different pattern densities, sputtering durations, curing times, and vacuum conditions that are critical in fabrication of CNTs are further examined. In this paper, we will study field emission properties. Randomly aligned Multi Walled Carbon Nanotubes (MWCNTs) are perceived as being the favorite types in industrial fabrication method producing CNTs. This is the facilitator of field emissions in the following device. The Carbon nanotube device is formed in multiple stages. The MWCNTs are grown with a pattern on a silicon wafer. The wafer is cut in smaller sizes and then with a metal perform the small section of the wafer with CNTs on is bonded to a ceramic package. A metal top plate is placed on the ceramic package and a gap is formed between the metal top and the MWCNTs. Then the entire assembly is permanently vacuumed sealed. Once assembled, a biased voltage is applied between the bottom and top metal plates. An electrode collects the emitted electrons from the CNTs tips, through the vacuum. The final assembled device is a small vacuum tube diode.

Acknowledgments

This National Science Foundation (NSF) research and thesis would not be possible if not for Dr. Kirkici, Dr. Dean and Dr. Baginski. Their mentorship during my time spent at Auburn University was greatly appreciated. All professors gave me laboratory space in the Electrical Engineering building, guidance, and fellow research peers.

The graduate peers I would like to thank are Baha Yakupoglu, Mike Moxley, and John Tatarchuk, for their help during the year of research dedicated to producing a Carbon Nanotube (CNT) vacuum tube Diode.

Another sincere salute of appreciation goes to my parents, my sister, aunts and uncles, my cat Sprinkle, my advisors (for letting me delay my thesis to grab a great employment opportunity), and my fiancée for their encouragement. (With everybody's help, I eventually finished this thesis)

One last thanks is directed to my friend from my undergraduate degree, Anthony Coulter, who had the time and patience to personally teach quantum mechanics, physics, and help me with this thesis. I will always be grateful to all those (even those that helped me to review this thesis) during this time.

This work is partially funded by EngeniusMicro, LLC, through a grant from the National Science Foundation NSF-STTR Program—Grant # G00007981.

Table of Contents

List of Tables

List of Figures

List of Abbreviations

AFM	Atomic Force Microscopy
CNT	Carbon Nanotubes
CVD	Chemical (Thermal) Vapor Deposition
DOS	Density of States
EELS	Electron Energy Loss Spectroscopy
ESR	Electron Spin Resonance
GSM	Graphene Sheet Model
LDF	Low Density Function
MPECVD	Microwave Plasma Enhanced CVD
MWCNT	Multi Walled Carbon Nanotubes
PECVD	Plasma Enhanced CVD
RFID	Radio Frequency Identification
RLC	Resistor, Inductor, and Capacitor Circuit
SEM	Scanning Electron Microscope
SWCNT	Single Walled Carbon Nanotubes
TEM	Transmission Electron Microscopy
WKB	Wentzel–Kramers–Brillouin

Chapter 1
Introduction

The Element Carbon

Graphite and diamond are the two main allotropic forms of bulk carbon. Fullerenes and carbon nanotubes constitute other allotropic forms. Carbon consists of layers (trigonally bonded) in which the carbon atoms are arranged in a honeycomb network. Distances between carbon atoms give different properties of the carbon allotropes. Such properties include, but not limited to: atomic density, specific heat, conductivity, compressibility, Band gap, electron mobility, hole mobility, resistivity, dielectric constant, dielectric breakdown, refractive index, defects, melting point, breaking strength (young's modulus), and morphology. Carbon has many allotropes including the following: Carbon fibers, carbon nanotubes (CNTs), carbon blacks, carbynes, carbolites, amorphous carbon, porous carbon, liquid carbon, graphite intercalation compounds, diamond, cage hydrocarbon molecules, metallo-carbohedrenes, and numerous carbon fullerenes. (A basic form buckyball or Buckminsterfullerene icosahedral molecule, C_{60}.)

Metal vs. Semiconducting Properties of CNTs

Examined in a solid state physics there are 3 basic types of materials. The first being no band gap where the valence band of electrons and the conduction band are overlapping. The next type has a small sized band gap (Si a typical semiconductor has a band gap of 1.12eV) where the conduction and valence band of electrons are completely separated. The last main type has a very large band gap between the valence and conduction bands. The valence band is the first filled

energy level and the conduction band is the last filled energy level. Intrinsic elements have a Fermi level in the middle of the band gap. N type material has a bias to bring electrons to the conduction band and a P type has a bias to have electrons stay near the valence band.

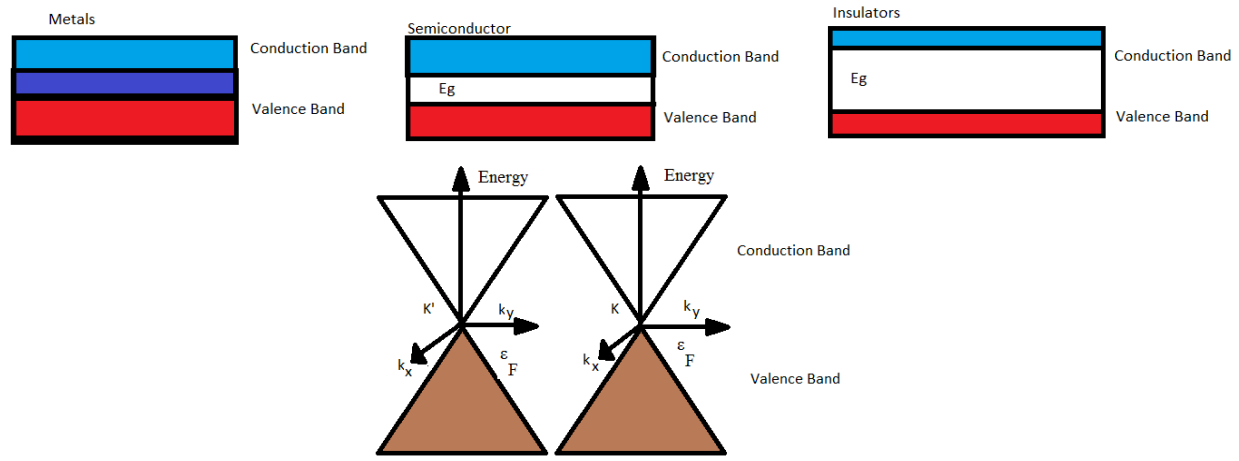

Figure 1.1 (top) Semiconductor band structure. (bottom) quantum structure with k and k' vectors with fermi level.

CNTs work more on a quantum mechanical level in which the electronic energy varies with its wavevector (k-vector in an envelope function). [1] According to Peng [2] a generalization to defining metal is a nanotube with a diameter less than .5nm. To characterize CNTs accurately the following properties need defining; diameter, curvature (armchair or zigzag), low density function (LDF), density of states (DOS), the graphene sheet model (GSM), and the dispersion relations of tubes in the vicinity of the Fermi level, ε_F. An electron in graphene is equivalent to a massless neutrino in two dimensions, and graphene therefore effectively realizes a system of relativistic particles moving with light velocity. The actual velocity of an electron in graphene is equivalent to about 1/300 of the velocity of light. Graphite is a semimetal that just barely conducts; only a few electrons can pass at one time to the conduction state. Varying some factors such as increasing the diameter of a carbon nanotube can

greatly impact its conduction properties. [3] When a finite band gap between the occupied states is known the material is a semiconductor but when there is infinitely small amount of space then carbon is now known as a metallic substance. These metallic carbon tubes become excellent field emitters.

CNT Classifications

Carbon Nanotubes (CNTs) are broadly classified into 3 categories; Single Walled Carbon Nanotubes (SWCNTS), Double Walled Carbon Nanotubes (DWCNTs) and Multi Walled Carbon Nanotubes (MWCNTs). Each category has its own unique characteristics and grown using different methods. A CNT has many varying parameters which include but are not limited to; tube diameter and wall thickness, tube length, number of layers on each tube, tip or root growth, tube density, and the type of helical pattern. In this Thesis, I synthesized and studied randomly grown MWCNTs. Therefore when referring to carbon nanotubes, it should be understood that the samples are all MWCNTs.

Synthesis of CNTs

There are many different methods to synthesize carbon nanotubes, and only the most commonly used few methods are cited in this Thesis. The final produced CNT samples used in this thesis were created with the use of CVD.

Arc discharge

Arc discharge is the first method for producing CNTs. The materials needed to do this process are two graphite electrodes, a power source of 12-25V and 50-120A, an inert gas with a vacuum chamber to contain the electrical arc. The test procedure involves the user to put the graphite electrodes into a vacuum chamber, bring down the pressure between 100-1000 torr, fill the chamber with an inert gas and produce electrical arcs between the graphite electrodes. This

process produces MWCNTs. [4] Iijima produced SWCNTs with a Fe:C anode in a methane: argon environment.[4] Bethune used a Co:C anode and He environment to produce SWCNTs. [5] Tailoring the diameter is directly linked to the gas mixtures. [6] The gas pressure affected the yield amount of CNTs. [6]

Laser Ablation Method

The laser ablation method produced samples of CNTs by the Smalley group. This group used a 2.5% Co 98.5% graphite target to grow CNTs. The target is placed in a 1200°C quartz tube furnace. The pressure is monitored at 500 torr with an inert gas of either He or Ar as the background gas. A continuous laser pulse from one end of the quarts tube reached the other end. The target catalyzes the growth of the CNTs. This method is used over the Arc discharge for a broader diameter range of the CNTs. The range varies between 1-1.6nm. [4]

Chemical (Thermal) Vapor Deposition (CVD)

CVD involves the process of gaseous carbon that flows over transition metal particles at temperatures between 500°C-1200°C at varying pressures of atmospheric, low pressure or ultralow vacuum pressures. This process can produce gram quantity bulk formation nanotubes, SWCNTs, MWCNTs, and vertically aligned MWCNTs in high atomic quality and high percentage yield. CVD growth is usually separated into 3 separate ordering schemes: growth mechanics, carbon gasses, and catalysts. [4]. In this Thesis, I used a thermal CVD method to synthesize CNTs used in the experiments.

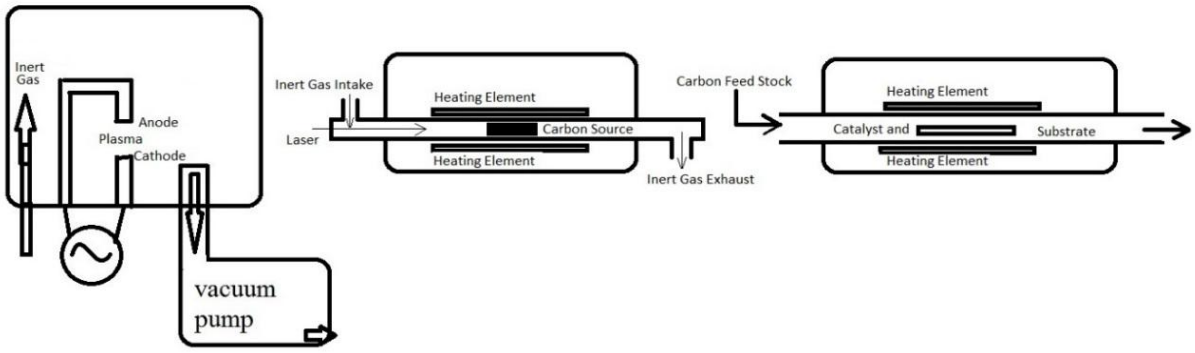

Figure 1.2 CNT production methods. (left) arc discharge. (middle) laser ablation. (right) CVD.

Microwave Plasma Enhanced CVD (MPECVD)

MPECVD is a technique to produce bulk (on a wafer between 2.0-7.5cm diameter) vertically aligned low temperature (under 500°K), low pressure (5-20torr) and good control of many growth parameters, except diameter. This source can produce vertically aligned MWCNTs and SWCNTs by the use of plasma produced by microwaves. Methane and ammonia are the most common gasses used to introduce carbon to the CNT mixtures.

Plasma Enhanced CVD (PECVD) (or Plasma Assisted CVD)

PECVD uses a heated substrate (500°C-800°C) in a carbon gaseous mixture at 500mTorr with a plasma coil sometimes in conjunction with an external magnetic field or hot filament. The plasma is used to help breakdown the carbon gasses into reactive carbon species. The carbon gasses commonly used are Methane, Benzene, Methanol, Ethylene, Acetylene and reactive carbon gases such as CH, C_2. The CNTs are grown during a vapor phase and this allows more variance in the usable substrates.

Notable Properties of CNTs

Most common features of Carbon Nanotubes include the following; structural, thermal, chemical, electrical, optical, and physical. CNTs have a larger than normal Young's modulus, is

as stiff as diamond and the estimated tensile strength is more than ten times that of steel wire with the same weight. It has even been suggested that nanotubes could be used to build a "Space elevator" which is an earth-to-space cable. CNTs are able to withstand regular temperatures well into the 100s°C and keeping good switching performance. The hole thermopower (Hall effect) is used to relate thermoelectric effects with the density of states (DOS). Where the parameters are k is thermal conductivity, T is temperature (measured in Kelvin), Density of states with respect to Energy, where n_s is the density of states per unit volume.

$$\rho(E)=\frac{dn_s}{dE}=\frac{4\pi(2m)^{3/2}}{h^3}\sqrt{E} \qquad [7]$$

$$S=\frac{\pi^2}{3}\frac{k_B T}{e}\frac{d(DOS(E_F))}{dE_F} \qquad [7]$$

Thermoelectric efficiency ZT where $Z=\frac{S^2\pi}{k}$ [7]

ZT enhancement is strongly correlated to an inverse proportion of electric conductivity and thermal conductivity. ZT plays a role in electron transport. Chemical interests in CNTs are centered on how they oxidize (gas or liquid phases) and how they react with gaseous mixtures. The covalent coupling with these mixtures can result in changing properties in CNTs. Such properties include the solubility, which dramatically reduce or grow the physical properties. (CNTs bonding with Aniline will increase the absorption rate. [8])These chemical reactions are amazing because they can bond chemically inert carbon to many different molecules. Electrical properties of interest are its electrical conductivity, field emission, small size, and use in high frequencies. Depending on mostly chirality the electronic properties can either act like a semiconductor or metal. By placing electrodes at different parts of the CNT, the resistivity was measured to be on the order of 10^{-4} Ω-cm at 27°C. The current density that was achievable was $10^{-7}A/cm^2$ but should be able to sustain much higher densities on the order of $10^{-33}A/cm^2$

[9]. With defects, a single CNT fiber can act like a transistor or a rectifier. These devices have been known to function at 10GHz. [10] Because of their sharp points (either open or closed tipped) the field emissions of CNTs are able to tunnel from the tip into a vacuum under strong applications of electric fields. [11] The optical properties are closely tied to the quantum level of physics and tensor calculations. The most useful quantities are the dielectric function $\varepsilon(\omega)$, dielectric displacement (**D**), Electric field (**E**) and the polarization, **P**. The biggest hampering factor faced by CNTs in optics is the bundling of fibers. This factor is responsible for a completely different absorption spectra and fluorescence. [11] Physical properties usually include the length, diameter and density of CNTs. Other physical properties including persistency, stiffness, and ruggedness can be unfurled by finding the correct chiral form. Bonding structures for the σ and π angles create types of CNT tubes; zigzag and armchair.

Measurement Standards and Techniques for CNTs

In the thesis research, we used SEM, profilometer, and Raman Spectroscopy to characterize CNT samples.

Scanning Electron Microscope (SEM)

The Scanning Electron Microscope (SEM) is a device that uses a beam of back scattered electrons to create an image. The electrons interact with atoms and create an image resolution of the sample from the vibrations with resolution to a nanometer. Higher vibrations appear whiter and lower vibrations appear darker. In certain circumstances colored SEM images are available with the help of a color look table. Energy beams from the electrons have an energy value usually between fractions of a few keV to 50keV. [12] The magnification is not controlled by power but rather by the current produced by the electrons. The scanning coils or the voltage applied to the deflector plates cause a magnification as high as several hundred thousand times in

magnification. Composition determination of several materials can be accomplished by using SEM. Biological, semiconducting, optical, and other material samples can be studies in a SEM. Most SEM devices coat the sample with a fine layer of gold before inserted into a vacuum. Other techniques have been used to observe living samples and ones with high humidity.

Atomic Force Microscopy (AFM)

The Atomic Force Microscopy (AFM) uses a cantilever, tip, piezoelectric element, a detector and a movable stage, and can take images up to fractions of a nanometer. There are 2 main types of AFM measurements namely tapping and tip oscillation (noncontact). The tapping mechanism uses the tip to measure out the peaks and troughs of the contours of a surface. The oscillating feature measures the electrostatic forces or VanDerWalls forces very close to a surface to get a topographical measurement. [4]

Electron Energy Loss Spectroscopy (EELS)

The Electron Energy Loss Spectroscopy (EELS) uses the energy loss spectra between empty and pea pod nanotubes (where pea pod is described as a hetrostructure; encapsulated fullerenes inside a nanotube). This method details the optical and electronic properties. The emission spectra is measured and can be calibrated in terms of eV and σ, π excited states. X ray diffraction is applied to determine the crystalline structure of the pea pod hetrostructures. [4] X ray spectroscopy often used to determine the density of states.

Raman Spectroscopy

Raman Spectroscopy is a technique used to measure charge transfer. Graphs are usually measured in energy (eV) versus distance (1/cm). Raman Spectroscopy is different than typical IR scattering because it can measure the resonance frequencies of materials. The laser light interacts with molecular vibrations, phonons or other excitations in the system, resulting in the energy of

the laser photons being shifted up or down. Raman bands arise from an oscillating dipole caused by light waves interacting with the polarizability ellipsoid of a vibrating molecule. [13]

Transmission Electron Microscopy (TEM)

Transmission Electron Microscopy (TEM) involves a beam of electrons going through thin objects interacting with in the substance as it exits. This equipment uses the de Broglie wavelength to examine the atomic structure of the substance. Bragg scattering is also considered to determine the morphology, find defects and analyze the crystal structure. [12]

Profileometer

A prifileometer is a calibrated device that measures the height of surface from origin. Destructive testing is performed during this procedure. The tip of the profilometer is dragged along a specified region in a straight line. The screen can show microscopic topology; bumps, craters and flat areas. Once complete with the tip dragging a screen shot is shown. If the tip was dragged over a bump or a valley then it will be seen along with measurements pertaining to height or valley. One area for improvement, is that the object under test needs to be fastened to a hard surface and the tip will not measure above certain heights without dragging the object under test.

Electron Spin Resonance (ESR)

An Electron Spin Resonance (ESR) is a device that measures materials with unpaired electrons. Using the Zeeman effect, the magnetic moment and the spin quantum numbers can be defined for a particular metallic or organic sample. ESR measurements are made with microwaves between the frequencies of 9-10 GHz and with magnetic fields in the region of 0.35T; thereby producing a spectral graph as a function of magnetic field strength (Gauss) and the frequency (GHz). [11] This graph can reveal the resonant frequency. The microwaves are

usually defined with a small pulse in duration of nanoseconds and used to control the spin characteristics.

Four Point Probe Measurement or Vander Paws

Four Point Probe Measurement (or Vander Paws) is a technique for examining PCB designs, micrometer device parameters and structures with different materials. This technique measures: resistivity, doping type, charge carrier density and the mobility of the majority and minority carrier. 4 criteria must be met in order to use the Vander Paw instrumentation. The shape must be flat, homogeneous, with uniform thickness. There cannot be isolated pits in the sample for test. The area under test must be at least an order of magnitude less than the entire sample. Certain characteristics can be taken; voltage, current, resistivity, conductivity, and Hall parameters.

Useful Applications

CNTs used in high frequency electronics, super conductivity, transistors, and sensors. High frequency electronics are created by a few processes but electrophoresis if small amounts of CNTs at a time can build small interconnects between electrodes measuring a few micrometers long with a very small diameter. An electrical current is directed through the CNT and the device will resonate at frequencies tested into the 60GHz and theoretically detected in the THz range [10]. Super conductivity of nanotubes has been studied. The length, diameter, and doping play an important role in super conductivity. Longer CNTs lead to super conductivity. Skinnier CNTs also lead to more super conductivity. High magnetic fields and high temperatures impair super conductivity [14]. CNTs have been used as materials in small thin transistors [10, 14]. They are used as very thin layer barriers for NPN junctions. CNT sensors have many applications because of their size, strength and tensile strength (Young's modulus). CNTs are

good candidates for sensors because of their ability to detect specific chemical elements and their ability to repel water. Bio Sensors differ in orientation in their electrical chemical formula. CNT-Oxidase Based Bio sensors include GOx,HRP, trosinase, laccase, asccase, and ascorbate. CNT Mechanical composites have many science fictional applications that one day may become reality. With the help of metal stinting, plasma spraying, thermal pressing, laser dispersion and electronic deposition we may be able to see a series of ropes fitted with CNTs to lead ships to low earth orbit. The ability to make high strength wearable materials is also a strong possibility. The most creative of all material composites is the strengthening of biological cells to prevent cancerous attacks.

Chapter 2
Fabrication of Carbon Nanotubes (CNTs)

2.1 Preparing Wafer Substrates in a Clean Room

All semiconductor fabrication procedures were performed in a 2,800 sf., class ~100 clean room. Users need to wear a bunny suit. (As seen in figure 2.1)

Figure 2.1 Yellow lighted lab used to preserve photoresist, align masks, use microscopes and cure wafers. Lab workers (not shown) wear bunny suits to keep particulates out of the air to keep effective PPM.

Step 1

Start with an entire N or P type wafer with a concentration in the order of 10^{20} atoms per centimeter cubed. The substrate has a polished and unpolished side. The wafer has an orientation of <100>. (See figure 2.3 for a top and side view)

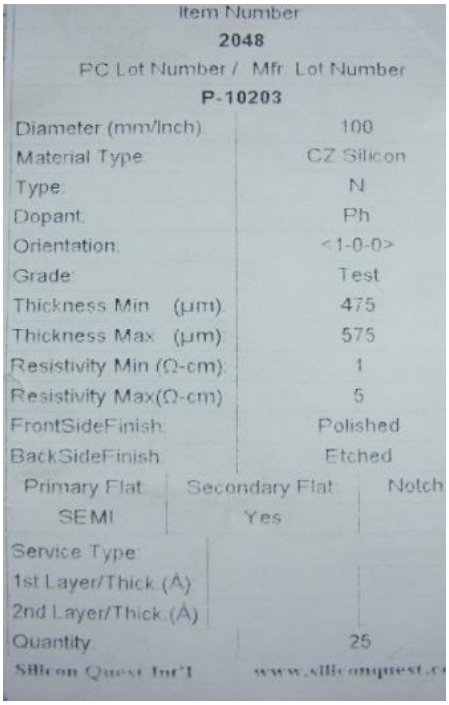

Item Number	
2048	
PC Lot Number / Mfr. Lot Number	
P-10203	
Diameter (mm/Inch)	100
Material Type	CZ Silicon
Type	N
Dopant	Ph
Orientation	<1-0-0>
Grade	Test
Thickness Min (µm)	475
Thickness Max (µm)	575
Resistivity Min (Ω-cm)	1
Resistivity Max(Ω-cm)	5
FrontSideFinish	Polished
BackSideFinish	Etched
Primary Flat / Secondary Flat / Notch	
SEMI / Yes	
Service Type	
1st Layer/Thick (Å)	
2nd Layer/Thick (Å)	
Quantity	25
Silicon Quest Int'l	www.siliconquest.c

Figure 2.2 A typical data sheet attached to the package of Si wafers. These wafers are bought from Silicon Quest International.

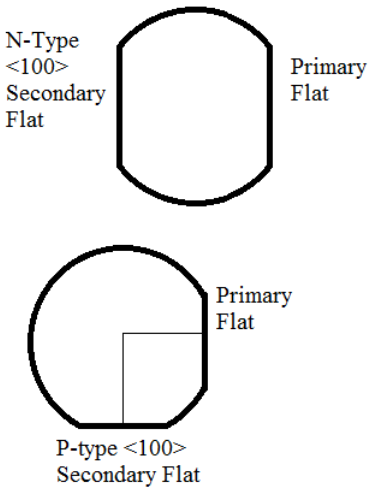

Figure 2.3 Substrate orientation for N or P type wafers.

Step 2

Cleaning the Silicon wafer: depending on the length that the wafer is exposed to the outside air, wafer surface is oxidized and collects particulates. That may make the wafer unusable. Silicon wafers, if not used need to be stores in a vacuum sealed container. A typical deep cleaning technique is mandatory for use before any fabrication process shown in table 2.

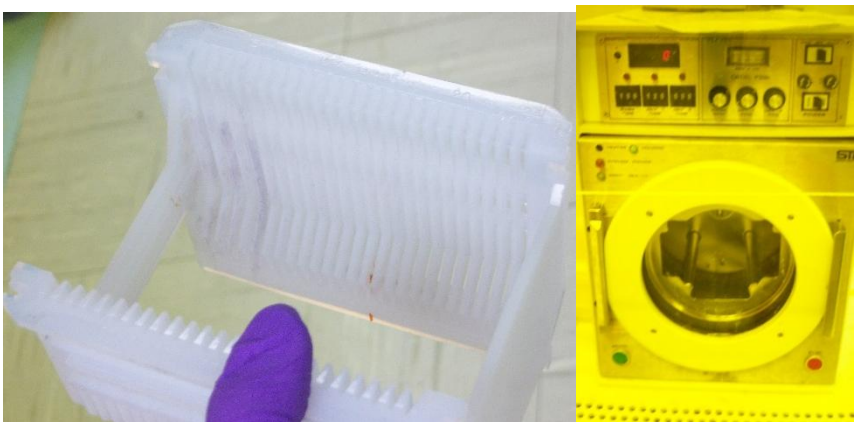

Figure 2.4 (left) A wafer storage during a distilled water washing process. (right) A machine to wash wafers.

If the wafers are not required to be rigorously cleaned it is commonly practiced to do step B, C and D of the RCA cleaning procedures. Then before applying the photoresist a dehydration bake the wafer to 120˚C for 20 minutes and HMDS vapor prime for 5 minutes.

Table 2.1 A deep cleaning with an RCA bath.

Silicon RCA Wafer Cleaning Procedure

A. Solvent Removal

1. Immerse in boiling trichloroethylene (TCE) for 3 min.

2. Immerse in boiling acetone for 3 min.

3. Immerse in boiling methyl alcohol for 3 min.

4. Wash in DI water for 3 min.

B. Removal of Residual Organic/Ionic Contamination

1. Immerse in a (5:1:1) solution of H_2O-NH_4OH-H_2O_2; heat

solution to 75-80 °C and hold for 10 min.

2. Quench the solution under running DI water for 1 min.

C. Hydrous Oxide Removal

1. Immerse in a (1:50) solution of HF-H_2O for 15 sec.

2. Wash in running DI water with agitation for 30 sec.

D. Heavy Metal Clean

1. Immerse in a (6:1:1) solution of H_2O-HCl-H_2O_2 for 10 min.

at a temperature of 75-80 °C.

2. Quench the solution under running DI water for 1 min.

3. Wash in running DI water for 20 min.

Step 3

Place the wafer on the CEE 100 spinner (seen in figure 2.5). Apply photoresist with a pipette to the middle of the wafer until ½ of the wafer is covered. The color of the photoresist is usually a dark red. The velocity and duration of the spin determines the thickness of the photoresist [15]. Once the photoresist is applied to the proper thickness the wafer is heated for 1 minute (baking stage).

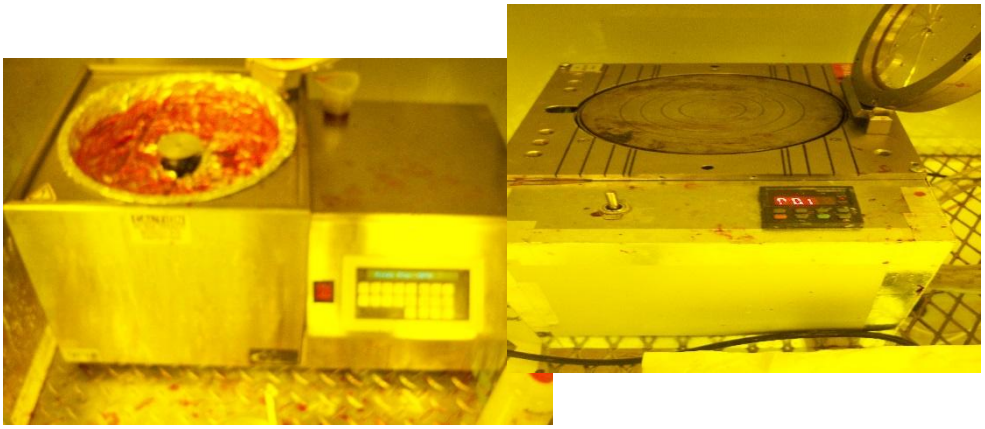

Figure 2.5 (left) Device to apply photoresist with a wafer already loaded. (right) After the wafer is coated with photoresist the wafer is cured.

Step 4

Mask alignment uses the Karl Suss Mask Aligner, (See figure 2.6), which performs high resolution photolithography. It offers unsurpassed flexibility in the handling of irregularly shaped substrates of differing thickness, as well as standard size wafers up to 6'' in diameter. It uses 5" masks System and it can be operated manually. All contact exposure programs (vacuum, hard and soft contact, and proximity) are provided to print structures far into the submicron region. X- and Y- shift are below 0.1µm and are not detectable by optical means. Wafers and substrates up

to 6 mm thick may be processed. The system is equipped with a Hg-Xe vapor lamp. The MA6 has upgraded optics designed to output in the mid-UV (250nm) range. The lamp is controlled by a CIC 100 constant intensity controller capable of delivering user-selectable UV doses which remain stable during the life of the lamp. Optical sensors monitor the UV output dose and provide feedback to the controller. There are 2 selectable channels. Both channels operate the lamp near its "idle power" (475W) to maximize lamp life. Because the lamp operates in constant intensity mode, the actual power will vary over time as the lamp ages.

Figure 2.6 The mask alignment system.

The wafer is vacuum sealed in the alignment system. The user checks the initial alignment in the monitor and adjusts the mask and the wafer. Once aligned the user hits the exposure button. The exposure time (high intensity UV light is shined onto the wafer) is on the

range of seconds. The exposure time should not be delayed more than 12 hours before the development bath. The negative mask is shown in figure 2.7. The UV light shines through the holes removing the photoresist.

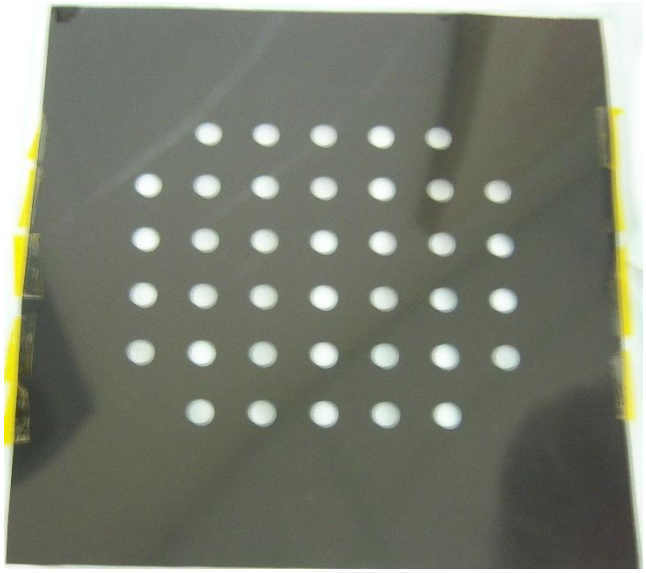

Figure 2.7 Mask on step 4. The experiment either used holes or rectangle shapes.

After the alignment the development bath is prepared for a 1 minute 3:1 H2O developer. The wafer is then rinsed in DI water and shaken gently then blown dry with a pressurized filtered air nozzle. The composition of the solution is 3 parts by volume DI water than 1 part volume AZ 400K solution. (150ml DI water and 50ml AZ 400K solution)

Figure 2.8 Area to obtain DI water from the faucet and dispose of AZ 400K solution.

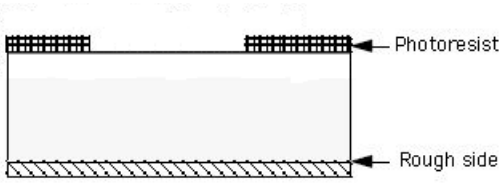

Figure 2.9 Status of the wafer after step 4.

Step 5

A hard bake is set to 120 ˚C for 20 minutes. This hardens the resist and improves the adhesion to the substrate. This stem improves the resistance of the photoresist to etchants. Plasma Descum with O2 is applied for 15seconds. The Plasma Descum has a mechanized arm

and programmed to take a certain slot wafer and bakes it. Table 3 summarizes wafer preparation.

Table 2.3 has a list of chemicals.

Figure 2.10 Plasma Descum furnace.

Cut Openings for Contacts

Dehydration Bake
Time **20 min**
Temp **120°C**

HMDS application
Time **5 min**

Photoresist application
Spin speed **3000 rpm**
Spin time **30 sec**

Softbake
temperature **105°C**
time **1 min**

Photoresist exposure
Mask used **No. 3**
Exposure time **10 sec**

Photoresist develop
Developer **AZ400K**
time **40 sec**
DI rinse **60 sec**
N2 dry -

Plasma Descum
Initial Pressure **O_2**
Time **15 sec**

Oxide Etch
Etchant Used **BOE 6:1**
Temperature **room temperature**
Time **1.5 min**

Table 2.2 Table to create a masked silicon wafer after a HF soak, DI bath, oxidation and HMDS treatment. BOE is used after the DC sputtering, annealing and CVD procedure is complete.

Table 2.3 A table of chemicals used for wafer preparation. HMDS, Sulfuric Acid, Hydrochloric Acid, AZP4620 Photoresist, AZ400K developer, Methanol and Acetone. Not shown are the HF, ammonia hydroxide, batch of BOE, and TCE. Please be careful around these chemicals.

2.2 DC Sputtering Deposition of Catalyst Material onto Substrate

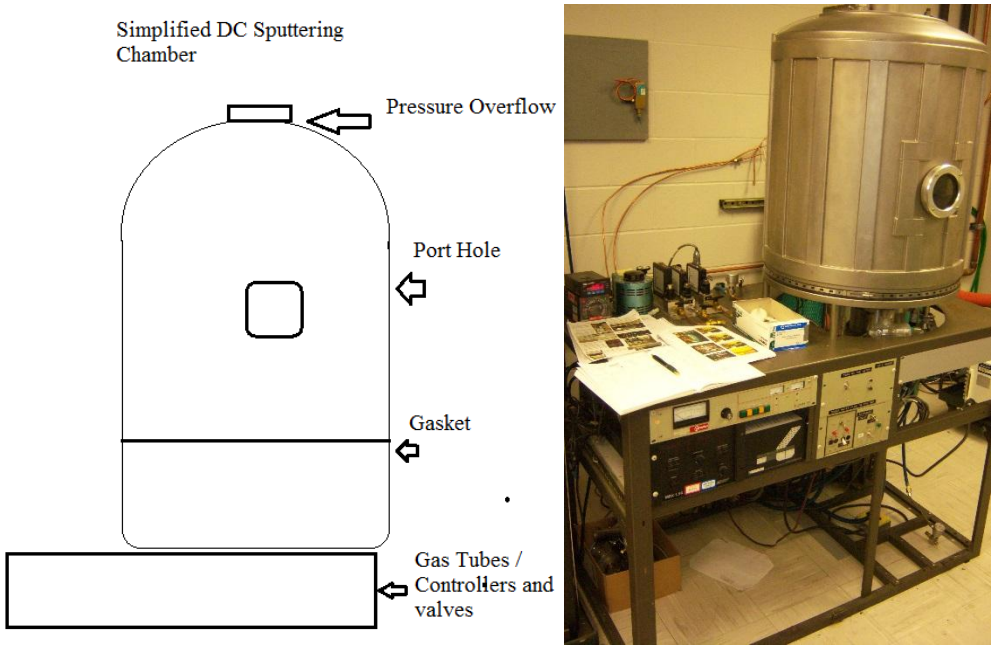

Figure 2.11 A simplified DC sputtering chamber example and real picture.

Sputtering Chamber Setup

Sputtering deposition is a method to form thin fills on substrates. This is a "physical" vapor deposition method where plasma is formed by a DC or RF power and the ionized atoms sputters target material. In the meantime the wafer is placed some distance from the target material and cooled so theta the atoms released from the target material are then "condense" onto the wafer surface. For this process a vacuum chamber with pressure control, DC or RF power source to generate plasma, and a selected target material is needed.

Step 1

The inside of the DC sputtering chamber must be free of debris from the last sputtering. A new sample (target) must be loaded into the chamber. The target is placed on a strong electromagnet called a magnetron. Below the sample on the magnetron is a disk with a small

hole. The chamber is brought down and a tight seal is made between the platform and the chamber. The pressue is reduced until $1*10^{-7}$torr [16].

Figure 2.12 (left) A disk where the sample sits with an adhesive. (We used a silver paste.) A small hole is drilled out so a gas can bombard atoms off the sample (middle left) which is placed on the magnetron (middle right) the substrate (right) prepared in the cleanroom.

Step 2

A MDX 1.5K Advanced Energy high power plasma generator warms up and ramps up to a high voltage and current. A gas is fed into the vacuum chamber. Our testing uses Argon in a constantly controlled proportion to flow next to the magnetron, sample and disk. The argon gas erodes the metal atoms off the target piece of metal onto the substrate. Depending on the duration of sputtering metal atoms onto the substrate, the distance from the substrate and sample, the amount of argon used to transport the metal, pressure and the power from the plasma generator a thickness of metal form is permanently bonded to the surface of the substrate with photoresist and negative shaped patterns. During sputtering measurements are taken. These measurements consist of the current, voltage, controller wattage, pressure of the chamber, amount of Ar gas used as transport, and the wafer type [17].

Time (seconds)	Power (Watts)	Voltage (Volts)	Current (Amps)
0 seconds	40 wats	367 volts	.07 amps
30 seconds	60 watts	380 volts	.12 amps
60 seconds	80 watts	386 volts	.17 amps
90 seconds	100 watts	393 volts	.22 amps
120 seconds	Open the protective plate for sputtering process		
XYZ seconds			

Table 2.4 The duration of deposited material, power, pressure, material, substrate type, and more information is kept in a log book format [16].

2.3 Annealing Substrate with Deposited Catalyst Material

Once the sputtering step is completed, a short agitated bath of acetone removes the photoresist and leaves shapes of deposited metal from the DC sputtering step. The acetone bath must be repeated several times with an agitated acetone bath, rinsing with methanol and then another rinsing with DI water. Once the wafer is completely cleaned, filtered pressurized air removes moisture. Verification of the work completed during cleaning is checked with a microscope. In this thesis we annealed the substrates within open air hot plate at 200°C at varying times [13]. Annealing is important in two ways. One is to eliminate oxidation of the metallic surface and the second is to form nucleation of metallic catalyst seeds to grow CNTs in CVD furnace. A better way of annealing is using a SST machine with the ability to remove atmosphere and particulates with heating elements. The preventing of oxidation to the carbon nanotubes eliminates most holes in the nanotubes and clustered particulates. Different annealing

times were also compared to emission data (see chapter 4, figure 4.3). Once the annealing step is completed a CVD process starts.

Figure 2.13 Annealing process alternatives. (left) A SST vacuum chamber with the addition of heating elements can cure substrates without the inclusion of particulates. (right) A hot plate with the sputtered and shiny side away from the hot plate.

2.4 Chemical Vapor Deposition (CVD) Process

The annealed substrate is loaded onto a quartz plate (boat). The quartz boat will sometimes have a lip to help keep the substrate from falling inside the CVD's tube. This lip needs to be carefully crafted. When the lip is too big, then it will block the laminar flow of reactive gases. We used acetylene 75ccm in our experiment is reactive and argon 22ccm is a transport gas. The pressure is calibrated along with the flow rate of gas and the temperature zone positions. The quarts plate with the substrate is placed into the tube and sealed. An amount of time varied for experimentation but the average time was around 30minutes at 705°C with .0013 torr of pressure.

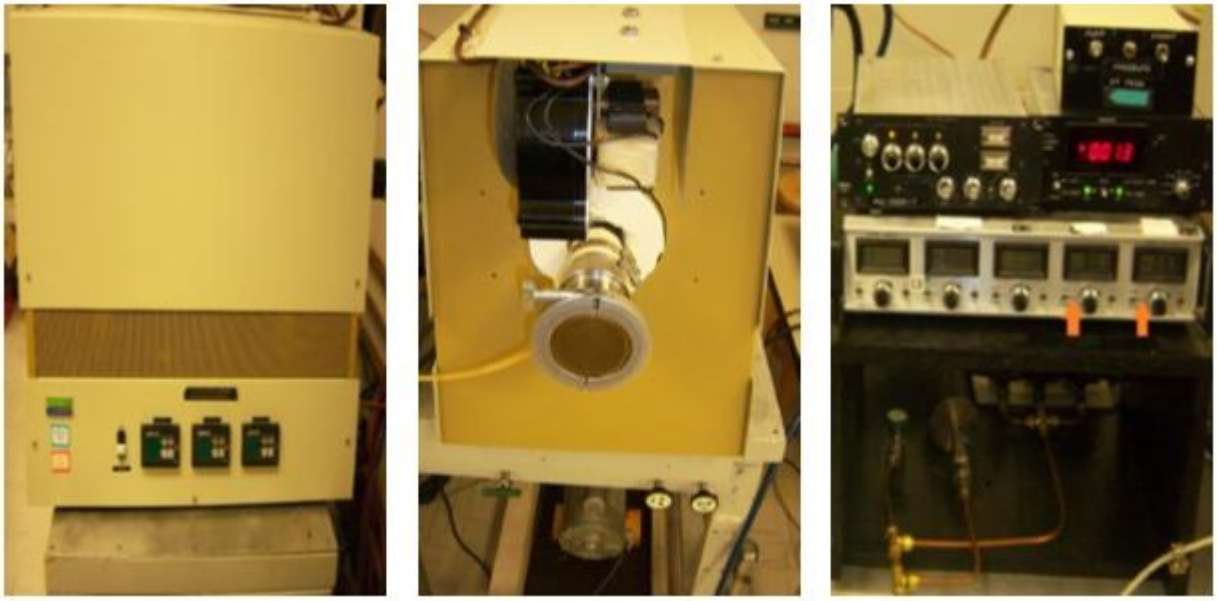

Figure 2.14 (left) controllers to control the temperature within the CVD. (middle) The metal tube clamped with a quarts ‘boat’ to hold the substrate. (right) gas controllers.

Chapter 3
Packaging and Making of a CNT Diode

3.1 CNT Vacuum Diode Diagram and Associated Properties

In a vacuum tube, electric current is carried only by electrons moving through the evacuated region (on the order 10^{-6} torr or less, without many collisions). The electrons in a tube are produced, literally, by boiling (700C-1000C) them off of the hot filament.[18] At this temperature, the average thermal energy of the electrons in the filament is larger than the electron binding energy, thus electrons are released from the filament. The binding energy will depend on the filament material.

The filament will produce a slight amount of electrical noise. In high quality low noise amplifiers, the filaments are usually heated with DC current thus requiring a secondary DC power supply. Vacuum tubes only have 1 noise parameter below the microwave region. Usually the effective input noise resistance, R_T of the tube is used to specify the noise generated within the tube according to: P_{ni}=4kTBR, $P_{ni} = GP_{no}$ where P_{ni} the effective noise at the input of the tube is, P_{no} is the tube noise at the output and G is the power gain of the tube [19].

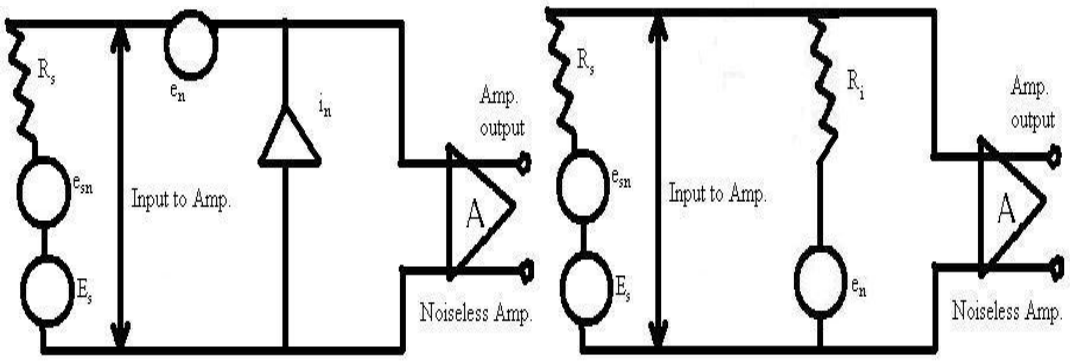

Figure 3.1 Transistor amplifier and source equivalent circuit (left), vacuum tube (right).

The vacuum tube diode consists of two electrodes inside the evacuated envelope. The cathode which is the filament wire plus oxide surface which emits the electrons and the anode plate collects the electrons [20]. For most vacuum tube diodes, the plate current increases almost linearly as the voltage difference between the anode and the cathode. A tube will also pass some current even when the plate cathode voltage is zero, because some of the electrons boiled off the cathode will have sufficient energy to reach the plate.

When the vacuum tube is compared to a Ge diode the turn on voltage between the p and the n side of the junction is about 0.30 volts regardless of the conducting current in a range of 1.0mA to 0.1A. Si diodes turn on at about 0.7 volts and this quantity is good for several hundred milliamps. [21] The vacuum diode turn on voltage is significantly higher. Since the vacuum diode is designed to withstand high voltages (in the range of 500Volts, but small current) the spacing between the cathode and anode must be bigger (to prevent breakdown), thus weakening the electric field.

The use of the vacuum tube diode is essentially the same as the semiconductor diodes. The basic principle of the diode is that it conducts current only in one direction. Only when the

plate is positive in voltage with respect to the cathode in a vacuum diode and only when the p-type material is positive with respect to the n type material in semiconductor diodes will the element carry current. Unlike the semiconductor diode the vacuum tube rectifier diode needs a secondary transformer winding to heat the filaments. LC filters in vacuum diodes are needed to reduce AC ripple, instead of a RC filter [19]. If the circuit is interrupted suddenly in either case the vacuum tube will take the transient surge; the material, junctions, and function will be destroyed.

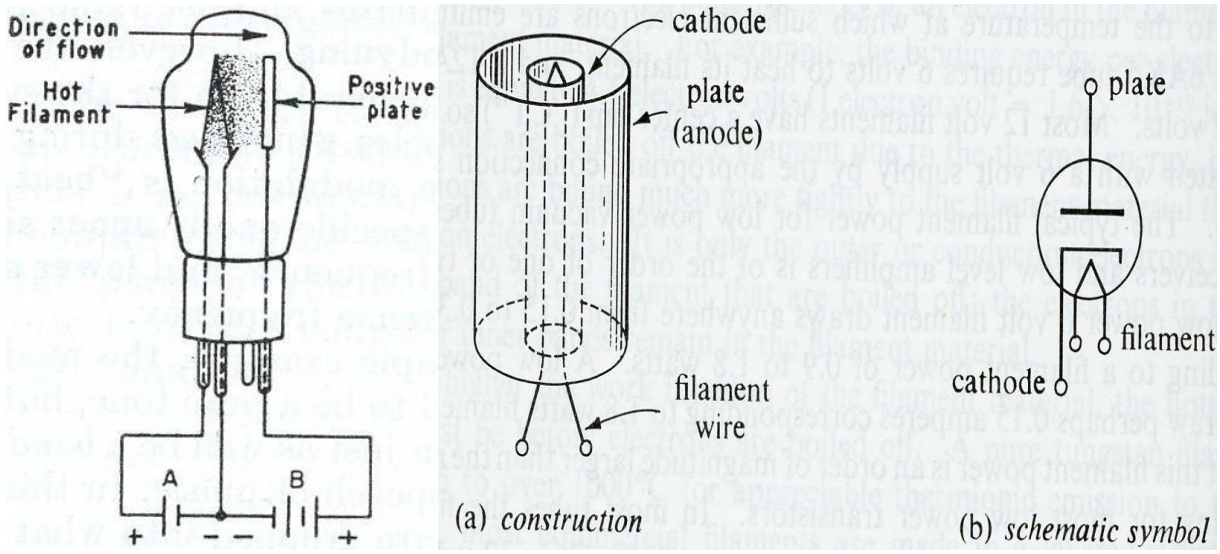

Figure 3.2 (Left) Physical Representation of vacuum tube. (Right) construction and symbol. [19]

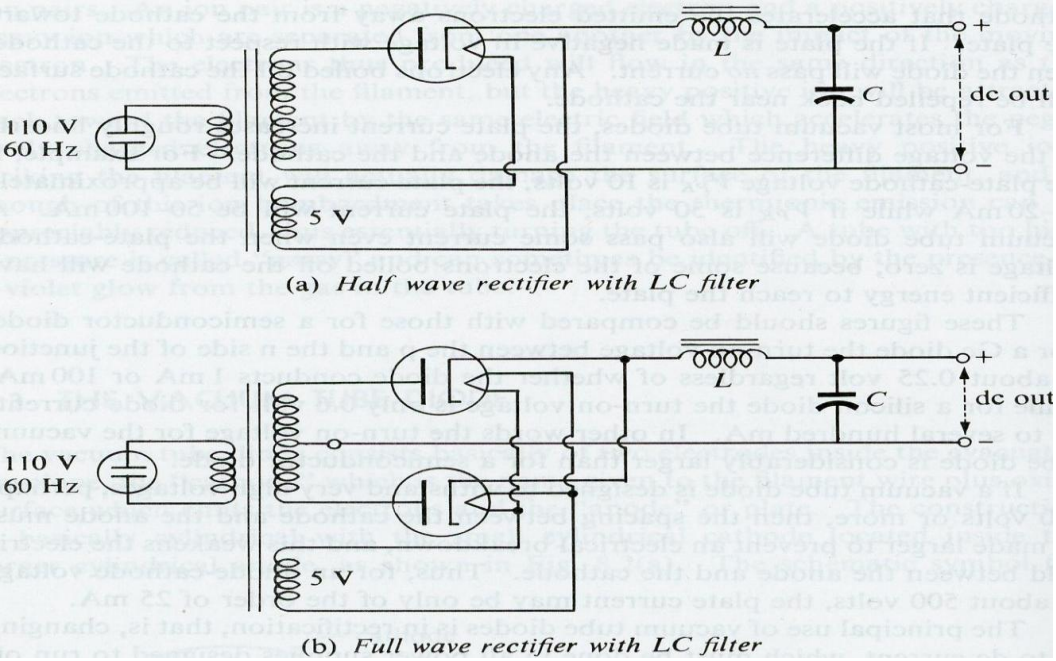

Figure 3.3 Vacuum tube power diode implementations in a half wave and full wave rectifiers. [19]

3.2 CNT Diode Assembly and Operating Characteristics

The diode is fabricated with particular attention to make a metallic bond to a ceramic back plate. The samples of CNTs grown on silicon substrate are cut either with a metal tong or a saw. The saw option is less preferred because of particulates generated during the cutting process. There are some creative ways to counteract particulates; such as taping a protective metal case with sealed top to the top of the CNT shape area. The finished piece (the CNTs sample) is around a 1cm square. Although in this thesis we used both n-type and p-type substrates to grow CNTs the thickness of the sample in this packaging configuration is 0.8mm P type silicon.

Figure 3.4 (top left) thin conductive sputtered metal on the back of the MWCNT shaped substrate. (top right) protective casing for the CNTs, produced with plasma etcher. (bottom left) finished cut squares with patterns used in the MWCNT vacuum tube diode. (bottom right) DC sputtering chamber within clean room used to sputter material for picture in top left.

The substrate has a sputtered conductive metal back and is placed on a thin gold perform (88% gold 12% germanium) on which all components are placed on the ceramic package. The protective casing with a top adorns the CNT sample. The assembled package is placed in a heated vacuum (such as the SST) at 300°C with a pressure of 10^{-5}torr. Pressure is applied to the protective casing to ensure a bond is made between the ceramic package and the CNT substrate with a gold perform. Then gold conductive thin wire creates a contact between the gold preform (located at the bottom of the device within the ceramic package) to the outside area out of the vacuum. This will act as the anode area. Once the substrate with MWCNTs are confirmed to be bonded to the ceramic package then the top lid is vacuum sealed with solder to the ceramic package in an atmosphere of 10^{-5} torr. The chamber was backfilled with nitrogen gas at 10^{-5}

torr. A mixture with a small concentration of hydrocarbons will provide the best performance to the device. The schematics of the device is shown in Figure 3.5. The device in figure 3,5 is the final vacuum tube CNT diode package. The thickness of the silicon wafer is predefined based on the distance of the vacuum gap of the anode cathode. Boding and flexing of the lid due to outside air compression on the inner vacuum. This boding can sometimes be as great as a few tenths of a millimeter in scale.

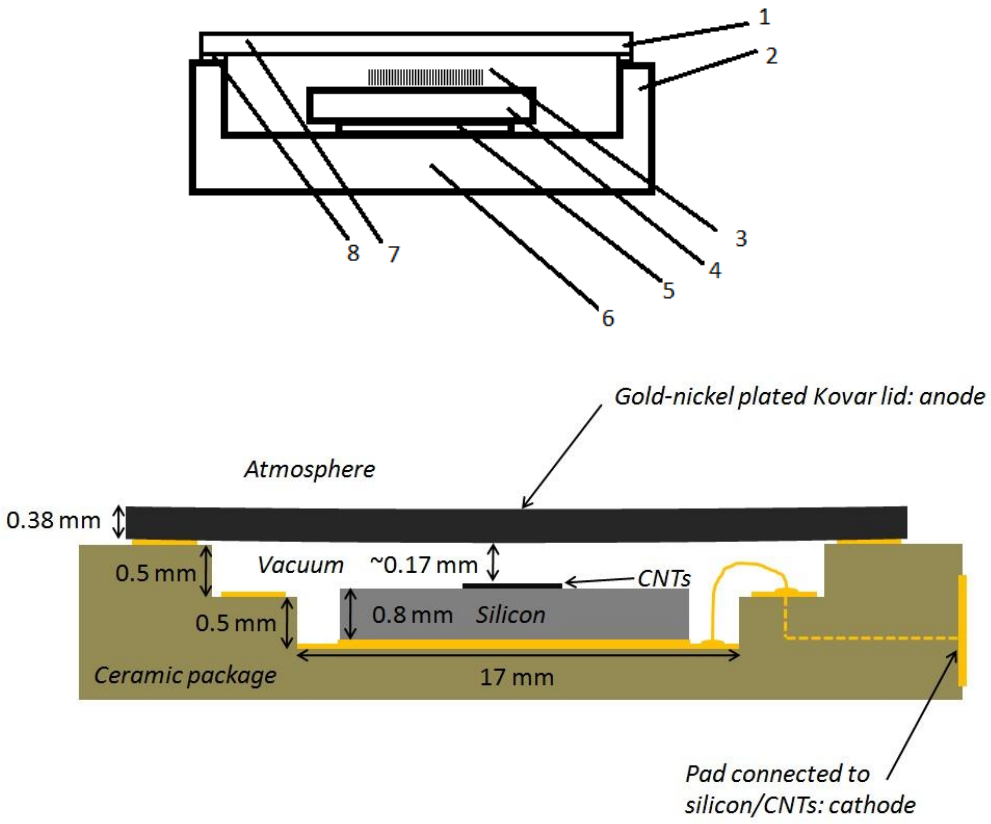

Figure 3.5 (top) Structure of the diode. Numbered with the parts for identification. (1) metallic lid. (2) ceramic package. (3) multi walled carbon nanotubes in a shape. (4) substrate. (5) thin gold metal performs. (6) ceramic package. (7) metallic lid. (8) metal solder used to create a sealed vacuum. (bottom) Another draft of the CNT vacuum package is displayed with measurements.

3.3 Fowler Nordheim Theory and Vacuum Tube Basics; Overview

Field emission is the process of pulling electrons from the surface of a conductor into free space with a strong electric field. The electric field between the plates of an ordinary capacitor will not usually suffice, but if one of the capacitor plates is replaced with a needle-shaped conductor whose tip points towards the other plate (hereafter called the anode), the electric charge at the needletip will be much stronger than in the parallel-plate case.

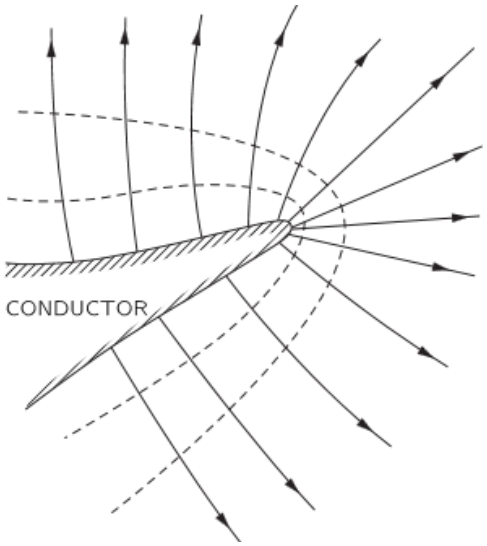

Figure 3.6 Shows the electric field and charge around an electric tip. [22]

If the field is strong enough, it will pull electronsΨ from the needle onto the anode. Millikan and Lauritsen [23] found empirically that the resulting current was proportional to $F^2 e^{-\frac{a}{F}}$ where F is the electric field strength in the gap and a is a constant that depends on the material type and the geometry. Fowler and Nordheim [24] derived the formula rigorously and determined the form of the constant a. We proceed with a simplified version of the Fowler-Nordheim derivation. An electron with energy E will have a quantum mechanical wavefunction that satisfies the time-independent Schrödinger equation

$$-\frac{\hbar^2}{2m}\nabla^2\Psi(x) + V(x)\Psi(x) = E\Psi(x)$$

where V(x) is the electric potential at position x. If V(x) is constant, then the electron is a free particle with energy E and it will have a wavefunction of the form

$$\Psi(\mathrm{x}) = \mathrm{C}e^{-jkx} \text{ with } k = \frac{\sqrt{2\mathrm{m}\,(\mathrm{E}-\mathrm{V})}}{\hbar}$$

If V(x) is not constant but at least varies slowly with x, then the solution will have a similar form but with kx replaced by

$$\int_0^x \frac{\sqrt{2m\,(E-V(\dot{x}))}}{\hbar}\,\mathrm{d}\dot{x}$$

which reduces to kx in the case that V is a constant function. This is the celebrated Wentzel–Kramers–Brillouin, (WKB) approximation [25]. Then if x=0 represents the tip of the needle and x=L is distance to the surface of the anode, then the ratio of the probability densities $|\Psi(\mathrm{L})^2|$ and $|\Psi(0)|^2$represents the likelihood that an electron at x=0 will successfully jump across the gap. Some algebra gives that this ratio as

$$\exp\left(-\frac{2}{\hbar}\int_0^L \sqrt{2m(V(x)-E)}\,dx\right)$$

This leaves the question of what potential to use for V(x). Since the needle is a conductor we can apply the free electron model to its interior. That is, all the energy levels in the needle's valence band are filled, the energy levels in the conduction band are mostly empty, and the energy E of a typical conduction electron will be the potential energy V(x) of the bottom of the conduction band[22]. Thus V(x)=E for negative x inside the needle. At x=0, the boundary between the needle's surface and the gap, the potential energy increases by ϕ, called the work function, which depends on the material and is responsible for holding electrons inside conductors. Between x=0 and x=L, the potential decreases linearly with a slope equal to the electric field. Locations with x>L are inside the anode and do not affect our integral. Thus V(x)-E = ϕ-Fex where F is the

electric field strength and e is the electron's charge [22]. Integrating the square root of this from 0 to L gives $\frac{2\sqrt{m}}{3e}\frac{\phi^{3/2}}{F}$ plus a negligible term. Substituting this result into the probability ratio puts the chances that an electron will tunnel at:

$$\text{Probability} = \exp\left(-\frac{4\sqrt{m}}{3e\hbar}\frac{\phi^{3/2}}{F}\right) \text{ [26]}$$

The resulting probability is proportional to the empirically measured current because our derivation made three incorrect simplifications. First, we supposed that only the most energetic electrons in the needle will jump to the anode, and so we treated E as a constant which was equal to the bottom of the needle's conduction band. But a strong field will excite lower-energy electrons as well, and a proper derivation will integrate over all the electron energies which are present in the metal; this correction puts the missing V^2 coefficient at the front of our expression. Our second error was neglecting the Schottky image effect [27]. When an electron is outside the surface of a conductor, it repels the electrons in the conductor and so leaves a positive `mirror image' of itself on the conductor's surface nearest the electron. When the electron is a distance x from the conductor its positive image attracts it with the force of a positive (but otherwise identical) electron at a distance of 2x. This effect reduces the potential by $\frac{e^2}{16\pi\varepsilon_0 x}$ so that $V_{corrected}\ (x) - E = \phi - \text{eFx} - \frac{e^2}{16\pi\varepsilon_0 x}$. The corrected potential is shown in the following image.

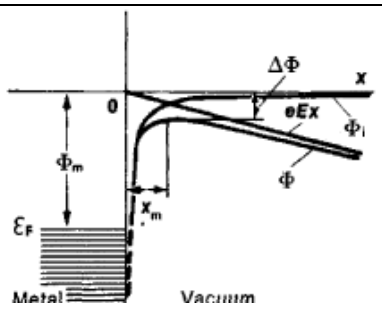

Figure 3.7 Diagram of the interactions between metal vacuum and sorrounding area.[24]

This gives a triangle potential and a rounded potential. The WKB approximation for this corrected potential was computed analytically by Burgess [28] and the complete formula is too complex to reproduce here. With these two modifications, the Fowler-Nordheim derivation matches experiments to within 15-20% over a wide range of voltages.

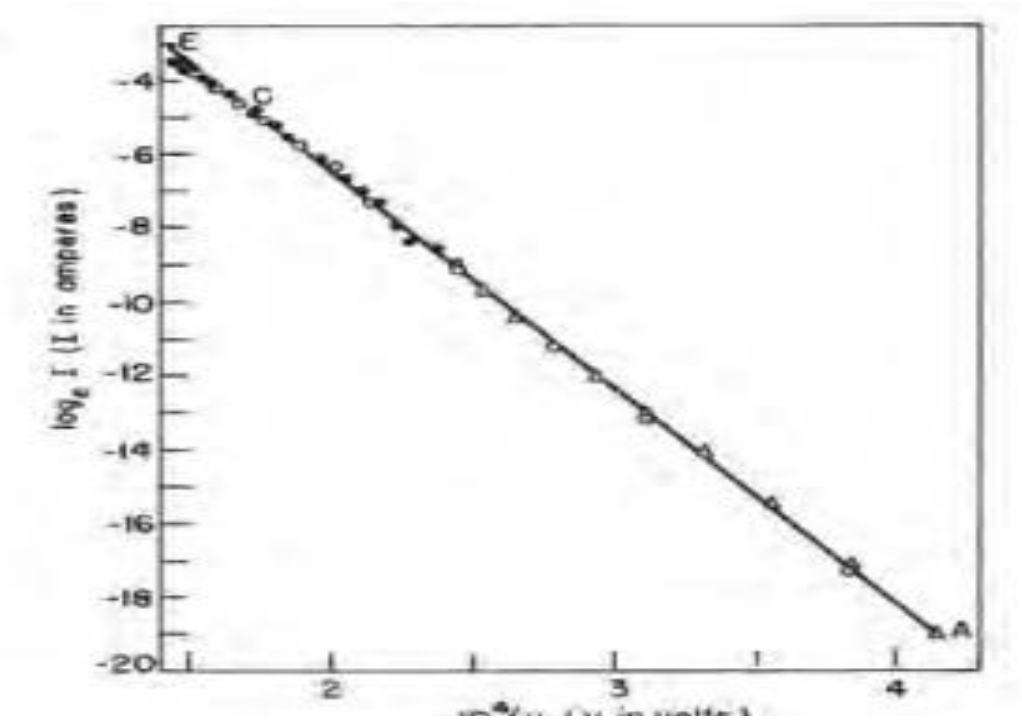

Figure 3.8 Experimental and theoretical current-voltage relations in field emission, from Dyke and Dolan [29]. Curve ACE represents the theoretical Fowler-Nordheim curve with image corrections in the exponent only. Experimental points: (hollow triangle), (hollow circle): DC; (filled circle), pulses. The deviation from the theoretical curve in the region CE is due to space-charge effects.

3.4 Fowler Nordheim Theory and Vacuum Tube Application

Carbon nanotubes field emission current from metallic surfaces is determined by the Fowler Nordheim equation.

$$I = aV^2 \exp\left(\frac{-b\phi^{\frac{3}{2}}}{\beta V}\right) \text{ [30]}$$

$$J = A\frac{(\beta E)^2}{\phi}\exp\left(-\frac{B\phi^{\frac{3}{2}}}{\beta E}\right) \text{ A=1.56}* 10^{-10}\,\frac{AeV}{V^2} \text{ B=6.83} * 10^3\,\frac{VeV^{-3/2}}{\mu m} \text{ [31]}$$

The variables in the above equations are 1 dimensional vectors and constants. Variables are defined by the following: J is the current density A/cm^2, I is the emission current , V is the voltage, ϕ (sometimes referred to as W and cannot be varied significantly) is the work function and is used as a constant at 4.7 eV, E is the applied field V/μm, and β is a normalized field enhancement factor. Metal's typical work function on a flat surface the threshold field is typically around $10^4\ V/\mu m$, which is high. [30] The larger the β the higher the field concentration and therefore the lower the effective threshold voltage for emission. [30] (Diamond has a very poor β value) Solving for β in the above equations is difficult and requires an iterative process. A solved solution required a Newton-Ralphson process. The solved equation (minus derivations looks like the following)

$$\text{Q} = \frac{1}{2}\ln\left(\frac{AE^2}{\phi \text{J}}\right),\ \ R = \frac{B\phi^{3/2}}{2E},\ \beta_{n+1} = \frac{\beta_n + R}{ln\,\beta_n + Q + 1}$$

From the data collected by the field emissions in a controlled vacuum chamber (seen in figure 4.2) we get the following sample graphs.

Field (V/micro-meter)	Current Density(A/cm^2)	1/Voltage	ln(J/v^2)
5.68	0.0038	176013	18.55
5.299	0.0037	188695	18.69
5.228	0.0033	191248	18.62
5.09	0.003	196215	18.58
5.02	0.0026	199006	18.48
4.89	0.0024	204498	18.43
4.78	0.002	208998	18.33
4.64	0.0018	215362	18.25
4.51	0.00153	221712	18.13
4.311	0.00133	231930	18.09
4.13	0.00109	241671	17.97
3.97	0.000855	251806	17.8
3.78	0.000637	264204	17.61
3.57	0.0004483	279605	17.37
3.34	0.0002885	298968	17.06
3.08	0.000168	324473	16.69
2.78	9.09E-05	358972	16.27
2.54	3.64E-05	393260	15.54
2.44	2.02E-05	408436	15.03
2.34	1.08E-05	425767	14.48
2.24	9.54E-06	445929	14.45
2.13	5.64E-06	467633	14.02
2.03	2.23E-06	491615	13.19
1.92	1.47E-07	518830	12.89
1.82	5.12E-07	549140	11.94
1.71	1.60E-07	583376	11
1.6	1.08E-07	622254	10.63
1.49	4.91E-07	666683	9.99
1.39	2.68E-08	717949	7.23

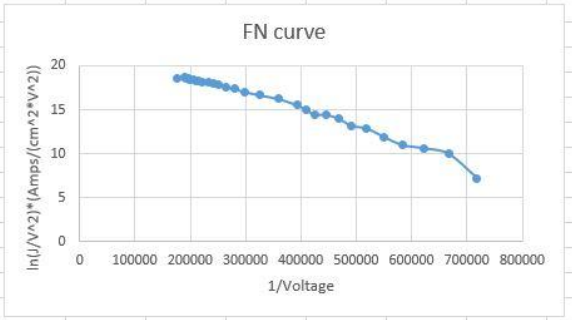

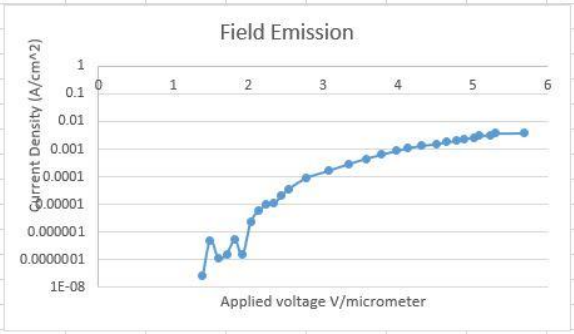

Figure 3.9 (data to the left) Raw data gathered from amps, volts, the gap distance referenced in figure 3.5, and anode area gives us the electric field, current density. (graph on the bottom) Field emission portrayed in a different manner. Turn on voltage is measured to around 2V/μm. (Graph on the top) F-N plot with a knee region (current pulse) [32] is seen at the second to last point.

Corresponding to figure 3.7, lowering the field emission threshold will increase the emitting current. Field emission current is mostly controlled by the external field. Electrons in solid material are confined by a potential energy barrier. The potential energy of a planer cold cathode with micro roughness can be written as the following equation.

$$U(x) = -\frac{e^2}{4x} - \beta eEx + E_F + \phi \text{ [31]}$$

The following variables are defined: U is the potential energy, x is the gap distance from anode to cathode, ϕ is the potential barrier for the electron, e is the charge quantity of an electron, and β

is a geometrical effect of microroughness on the electric field, crystal structure, conductivity, work function and nanostructure density. [31]

Doping can also improve the performance of CNTs by reducing the work function. Lowering the electron barrier is beneficial to the field emissions. The relationship between the electron concentration and the Fermi Level can be written as the following equation.

$$n = 2\left(\frac{2\pi m^* kT}{h^2}\right)^{3/2}\exp[(E_F - E_C)/kT] \text{ [31]}$$

The value n is the electron concentration, m* is the effective mass of an electron, k is the Boltsmann's constant, h is Plansk's constant and T is an absolute temperature in Kelvin. E_F is the Fermi energy level and E_C is the energy at the conduction band. Negative electron affinity can be very advantageous for electron emissions. [31]

Chapter 4
CNT Diode Testing

4.1 Field Emissions Testing

During fabrication of the CNT diode field emission testing of CNTs in vacuum is performed. First test area is on a sample of CNTs with substrate. The I vs V curve is compared and samples of a batch of CNTs are picked to create a diode package. In a batch of CNTs the yield is around 6-8 shapes with dense black MWCNTs. The next sample is used with a bonded ceramic package, gold lead and anodes and cathodes. If the sample is still shows good field emissions (turn on voltage around 400V/μm) we continue testing until full completion.

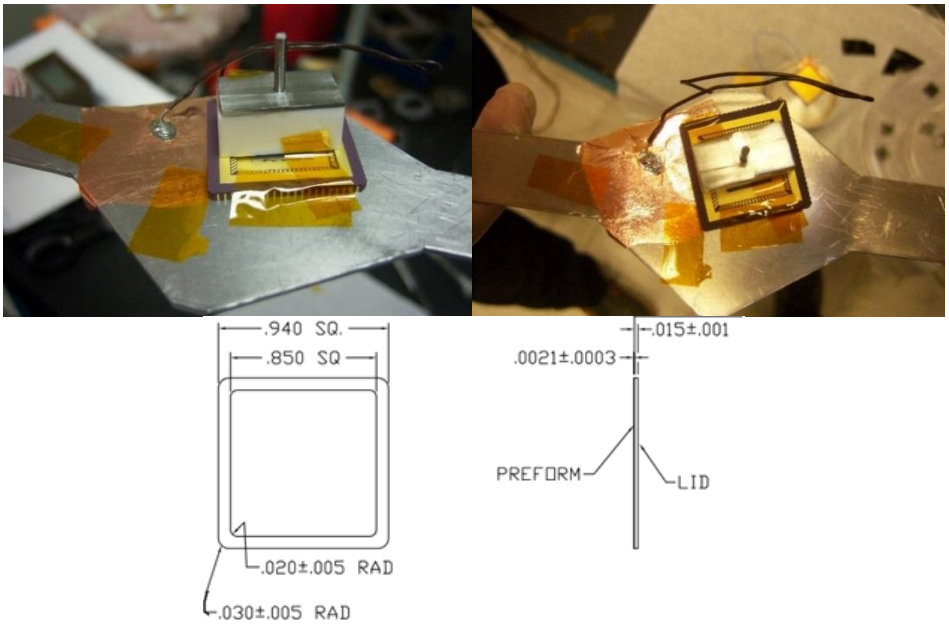

Figure 4.1 (top) a prototype diode setup for field emission testing with pictures of top and bottom sides. (bottom).Dimensions in cm of the ceramic tile used in the final vacuum tube diode. Dielectric tape with thickness of 250 μm separates the CNTs from the cathode.

A sample of the substrate with MWCNTs are placed on a conductive sheet and put into the vacuum chamber. The vacuum chamber has a high voltage feedthrough on the bottom that is connected to the programmable high voltage(up to 1500VDC) power supply. Another high voltage feedthrough that is positioned opposite to the previous one serves as lead to the anode and takes the current readings. The voltage and current data is collected by a GPIB interface and automatically plotted on a Matlab GUI from raw data points [33]. The automation has variable parameters for the amount of voltage starting and stopping, the rates of voltage increase and time between measuring sample data. The automation looks for a voltage stability, collects voltage and current ratings and parses them into 2 columns. These columns collect both charging currents and voltages and discharging currents and voltages. The discharge field emission is expected to show a slower moving slope and curve of the graph that was created during the charging stage [34]. These columns are analyzed in Microsoft excel and plotted for incoming current density and the applied field. This field emission data was able to verify that the data for a fully formed diode rectifies for reversed biased conditions.

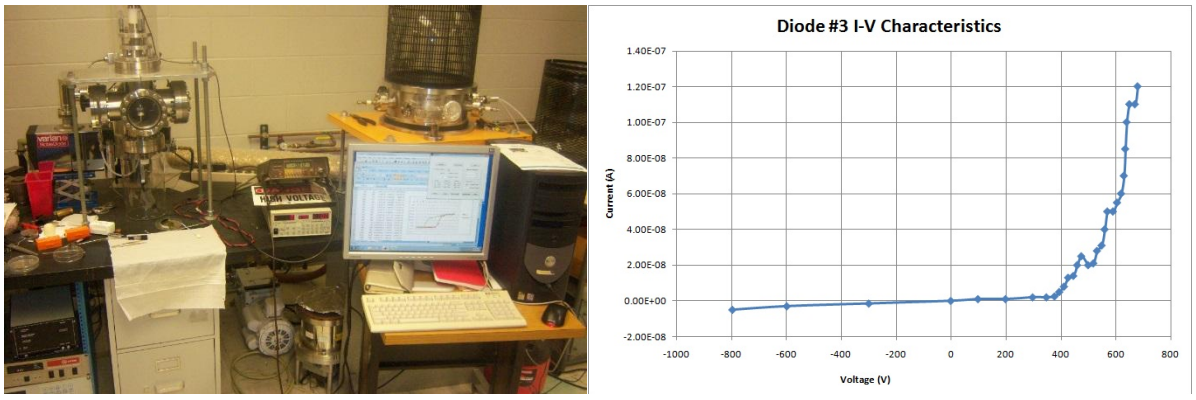

Figure 4.2 (left) Field emission vacuum chamber, amp meter, voltage source, GPIB communication signal with MATLAB GUI interface. (right) Field Emission from a fully packaged CNT vacuum tube.

During the fabrication of the substrate phase of this experiment the CNTs have varied times of exposure to annealing, DC sputtering and CVD processing. Per the appendix picture section of this thesis there were some DC sputtering durations that did not produce CNTs. The amount of iron sputtered onto the silicon substrate was either too thin or thick to produce CNTs. Profilometer measurements are calculated to be in the micrometer range for DC sputtering. As a general rule for testing each minute of the parameters; 100W DC power, about a 1.5 foot target to substrate distance, iron target, gas proportion, and vacuum condition, increased the iron height 0.2-2 micrometers. This variation depended a great deal on the state of the iron target, how much had been depleted from previous sputtering. The target depletion state also coincided with the data in Table 2.4 for voltage and current values used to get 100W. After annealing in a covered open air environment there were some oxidation present (rust). After annealing, the height of the iron on the silicon wafer grew. In the SST there was no evidence of oxidation after annealing, thus the iron on the silicon grew less. Cleaning silicon with bonded iron with methanol or acetone after annealing (but before CVD process) did not increase or decrease the yield of CNTs. CVD duration also had a testing procedure to determine the best recommended practice. In general, CVD duration is successful from 15-25 minutes. Durations of CVD exposure before 15minutes and after 25 minutes did not produce good yields of CNTs. After testing many variations the best recipe for growing CNTs was at 5 minutes sputtering, 8 hours of annealing in the SST vacuum 10^{-5} torr at 300°C and 25 minutes of CVD with argon and acetylene at 22ccm and 75 ccm respectively.

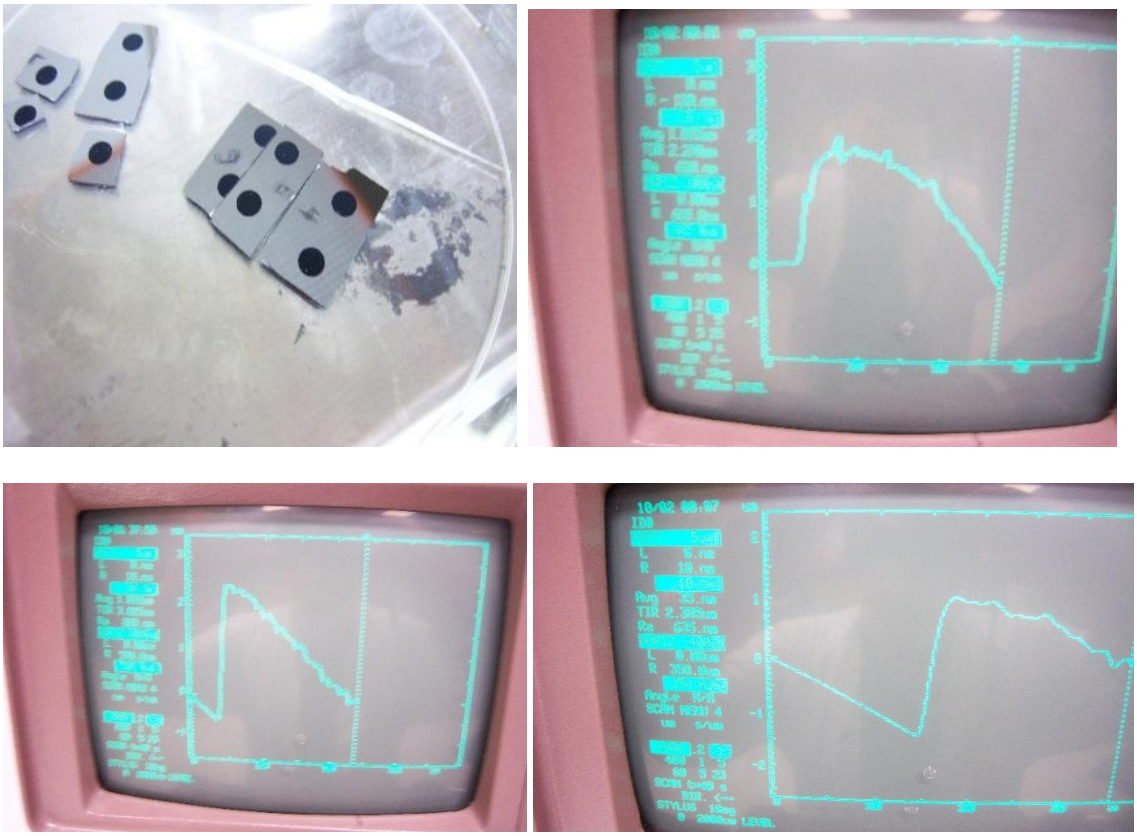

Figure 4.3 (Top Left) Wafers with 4, 5, and 6 hours of annealing at 315°C in a vacuum provided in a SST machine. (Top Right) Profile reading of the 5 hour annealed sample. CNTs grew to 2µm. (Bottom Left) 2.5µm height of CNTs at 6 hour annealing. (Bottom Right) 1.5µm height of CNTs after annealing for 4 hours.

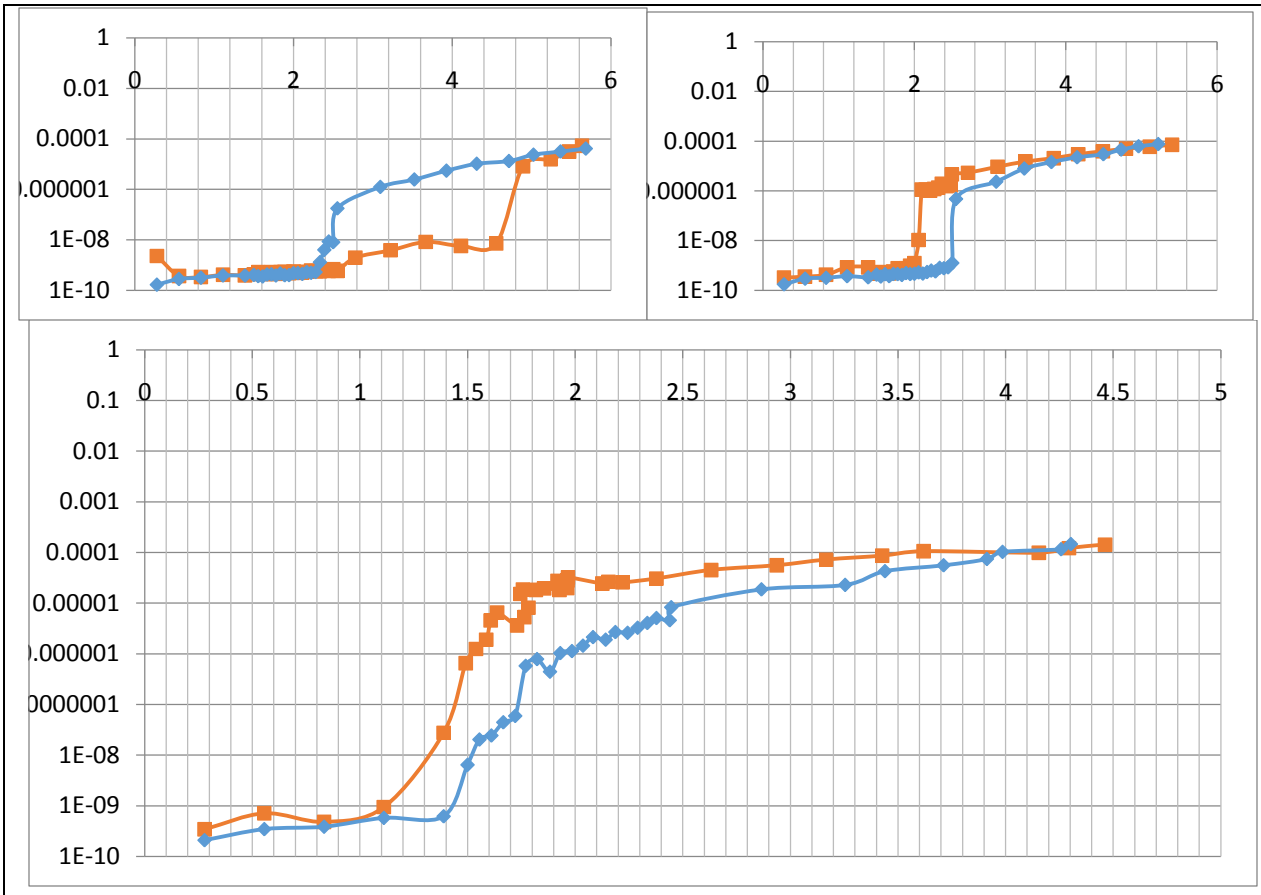

Figure 4.4 All graphs have separated with colors initial charge and discharge colored red and blue respectively (Top Left) Field Emission from 4 hours of annealing, turn on voltage is around 2..5V/μm^2. (Top Right) Field Emission from 6 hours of annealing, turn on voltage is around 2.0V/μm^2. (Bottom) Field Emission from 8 hours of annealing, turn on voltage is around 1.5V/μm^2. Annealing at 315°C in SST chamber.

4.2 CNT Diode; RFID Tag Testing

The fundamental design of the RFID tag is an RLC circuit. [35] In a series RLC circuit the current through each element is the same in magnitude and phase. By Kirchhoff's voltage law, the voltage V_{in} must be equal to the instantaneous sum of the voltages across each of the elements (i.e. capacitor, inductor and resistor). The phase of the current relative to the applied voltage is given by $\theta = \arctan\left(\frac{\omega L - (1/\omega C)}{R}\right)$. If $\omega L > (1/\omega C)$, the current leads the applied

voltage by θ. In the case of parallel combination of *L* and *C*, the impedance is $Z = \frac{j\omega C}{1-\omega^2 LC}$ and the phase of the output voltage relative to the input voltage changes by 180° as ω passes through ω_o (*resonance*). In a parallel circuit, resonance occurs when the impedance approaches infinity and the current goes toward zero and the voltage converges to a maximum. This is the opposite in the RLC series circuit; voltage is at minimum, current is at a minimum and a phase at zero (see Figure 4.5). The resonant frequency equation that satisfies both parallel and series is given by: $\omega_0 = \frac{1}{\sqrt{CL}}$.

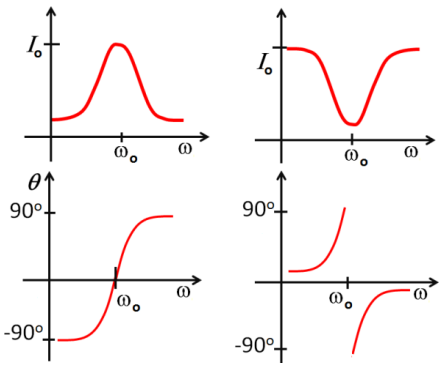

Figure 4.5 Sketch of phase parameters and resonant points for series (left) and parallel (right) RLC circuits showing the resonance point for current (top) and phase (bottom) parameters.

This paper pays attention to the parallel RLC circuits because of their ability to tune to a specific frequency by contrast series RLC circuits attenuate narrow bands around the resonant point. Depending on the circuit parameters, an RLC circuit is said to be over-damped if ($\alpha^2 > \omega_o^2$), critically damped if ($\alpha^2 = \omega_o^2$), and under damped if ($\alpha^2 < \omega_o^2$), where $\alpha = \frac{1}{2RC}$ [36]. In terms of the circuit under test in our experiments, the underdamped example will be examined.

Figure 4.6 shows the test setup for determining the operating parrlcameters of both a pn-junction diode and the CNT diode as an RF-sensor. A 250MHz pulse generator is connected to a transmit antenna as well as an oscilloscope. The biconical antennas, from ETS Lindgren, have a wideband frequency range of 20MHz – 300MHz and high input power capability of 3kW. These antennas are used as a transceiver and receiver. The RFID tag's coil is pulled through a Pearson coil which reads the RFID tag's current signal. Once the signal is launched, the amplitude, frequency, and FFT of the signal are recorded by the oscilloscope. The signal has a maximum frequency of 200MHz, and a peak current of 500A. The RFID tag is placed in range of the transmitting antenna and its resonance is picked up by the receiving antenna. The receiving antenna has the signal from both the transmitting antenna and the RFID tag (see Figure 4.6)

First a general purpose pn-junction diode is used to qualify the system parameters. Then the same test-bed setup, including components listed above, is used when testing our CNTs diode. One exception is that the CNTs diode is placed in a vacuum chamber and a curve tracer is used to record the diode performance. For that a bell jar vacuum chamber which is capable of maintaining pressures lower than 10^{-3} torr is used. This is because, the CNT-diode operates based of field emission electrons as a function of applied voltage. The CNT diode turned on with a high power pulse generator connected to the biconical antennas. The curve tracer is used to add any additional voltage to get an operational state and measure turn-on-voltages of the CNT sample.

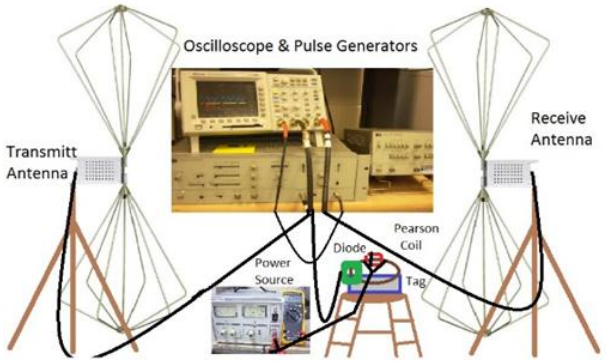

Figure 4.6 Schematic of the Test setup for both the general purpose pn-junction solid state diode and CNTs diode were tested for their turn on as a passive or active RFID tag.

There are two areas of manual testing performed to qualify the test-bed. One if to find the best RFID tag for use in CNTs measurements. For that, six RFID tags were created from 22awg wire with polymer insulation. The manufacturing of RFID tags will help determine the overall frequency of the tag [37]. Pictures of the two of the tags are shown in Figure 4.7. These tags have unique characteristics concerting length of the coil and number of loops. Each tag has the same initial capacitance of 0.192 microfarads, constructed from 5 equal capacitors in parallel and a diode in parallel.

Figure 4.7 Two of the RFID tags tested for performance based on the 90° of bandwidth. The antenna's sizes are; 120cm, 84cm, 380cm, 23cm, 205cm, and 25cm. The lower RFID tag is the one chosen to have the best performing and used in testing the CNT diode.

In order to choose the best RFID tag, each tag is characterized using a pn-junction solid-state diode. Particularly interesting in near field communications involving RFID tags are opportunities to find potential dead zones [38]. A dead zone is a place where a communication signal should be strong but found to have little signal. A coordinate system of 25 points (5 x 5 grid) and 90° of aperture was marked on the ground. Each point was measured 1 meter increments. The transmit antenna was at the bottom corner of the coordinate system labeled (0,0). It had a constant transmitting voltage of 8 volts and 25MHz. The RFID tag under test has its voltage measured with the Pearson coil. All tags had a measured capacitance of 0.192 microfarads (value measured at 1kHz) in series with the pn-junction solid state diode. It is concluded that all tags were operational and that had a VSWR that decreased in proportion to $(1/R^2)$. Once the data is recorded, a plot of each RFID tags is generated using a MATLAB code. Figure 4.8 shows the plots of best and worst performing tags.

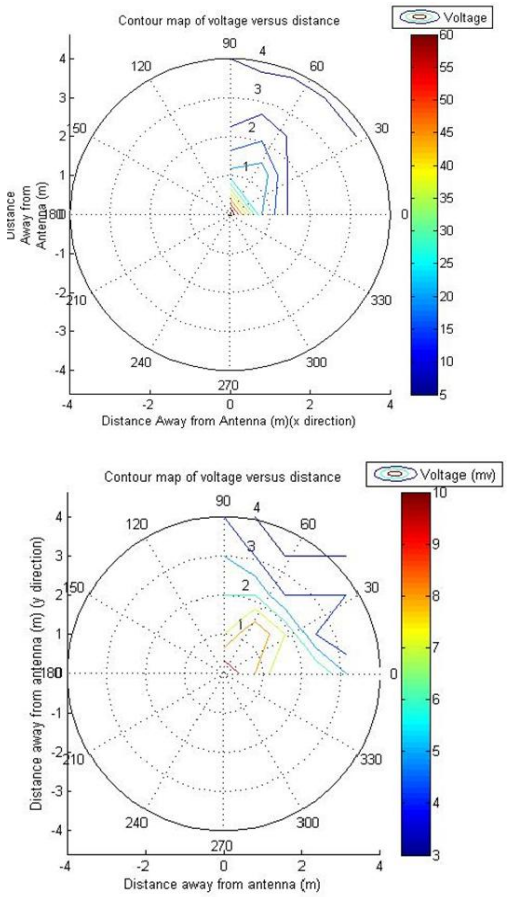

Figure 4.8 MATLAB plots of the 90° of recorded data for the potential field for the best (bottom) and worst (top) performing RFID tag. Top plot is the weakest tag and at the transmit antenna has a voltage of 10mV. Bottom plot shows the strongest tag at 60mV at the transmit antenna.

The test-bed is characterized in passive and active mode. The RFID tags are used with the general purpose pn junction solid state diode first. Figure 4.9 shows the oscilloscope plot of transmit and receive antennas as well as the current reading from the Pearson coil. The transmit antenna generates an 8V signal with 25MHz on channel 1. On channel 2 the current detected by Pearson coil is displayed, showing an underdamped characteristic. On channel 4 is the signal from the receive antenna, which also has underdamped characteristics. The "M" channel is a FFT of the Pearson coil signal [39]. From Figure 4.9, one can see the harmonics at 25MHz

intervals and a resonance frequency at 25MHz.

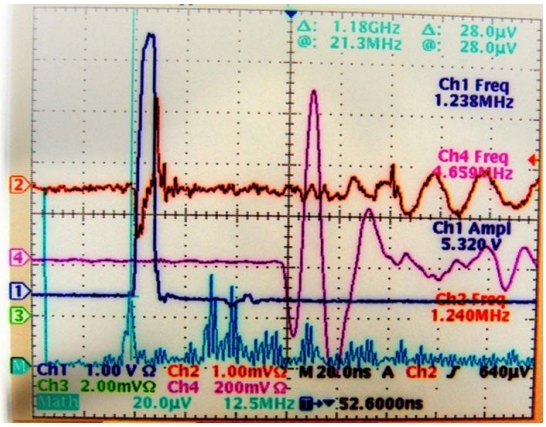

Figure 4.9 The pn-junction diode test-bed oscilloscope screenshot.

If we use the diode equation $I_D = I_S \exp(V_D / V_T)$ and by substituting a frequency dependent voltage, $V_D(f)$ in this equation, we can express the equation using Taylor expansion. Then the harmonics and the resonant frequency of the RFID tag can be determined [40]. In this study we have determined the harmonics at 25MHz intervals and a resonance frequency at 25MHz, as shown in Figure 4.9.

In order to test the CNT diode, we first made a "sample" holder for the CNT-diode. A ceramic plate with the dimensions of 1" x 3" x .25" is used to hold the CNTs substrate and the diode assembly. Four holes are drilled 0.25" away from the corners and long metallic screws are used to hold the plates together. Copper (Cu) sheets are located on either side of the ceramic blocks and the CNT diode is placed between the ceramic plates. The Cu sheets are extended over the side of either ceramic plates and had enough area to make contact with the diode. CNT sample is placed on the bottom ceramic plate on the Cu sheet facing toward the top plate. The 140 μm thick glass spacer is used either side of the samples to determine the distance as in the field emission tests. The anode is placed over the CNTs and making contact with the glass

spacer. And image of the CNTs sample used in constructing the diode and the diode-housing are shown in Figure 4.10. The fabrication details of the CNTs samples are presented elsewhere [41].

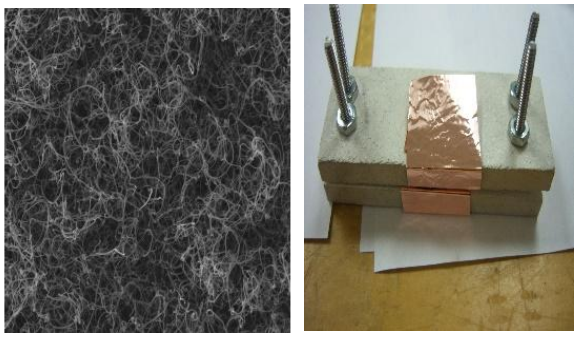

Figure 4.10 Image on left is the SEM image of a CNTs film grown in CVD chamber after 5 micrometer thick Fe catalyst layer is sputtered. Image on right is the ceramic plates containing the CNT-diode sample.

Current-voltage (IV) characteristic of the CNT diode is recorded with a Tektronix type 177 curve tracer as shown in Figure 4.11. The IV curve shows a cathode to anode current and an anode to cathode voltage. The figure relates the voltage and current operating point. The straight line is called the load line and the intersection of the load line and the I-V characteristics gives the operating point of the diode.

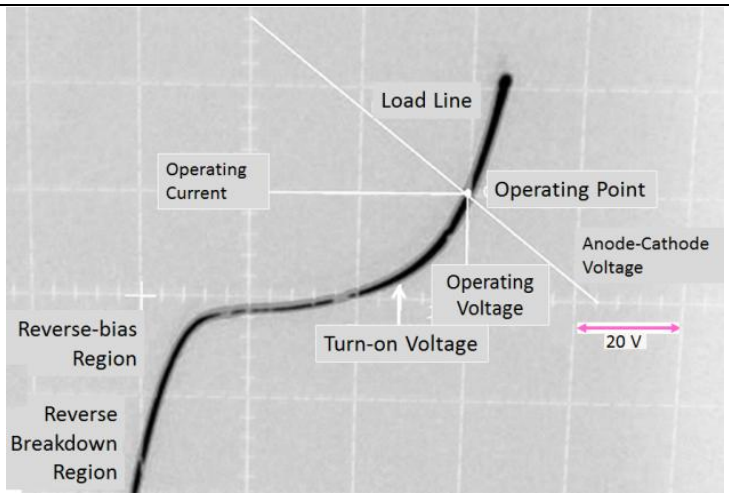

Figure 4.11 Current versus voltage curve with labeled parameters.

Figure 4.11 shows the screen capture of the CNT-diode performance under pulsed RF field. The frequency of the electrical pulse that is fed into the antenna is 91 MHz. Transmit antenna has 5 volts and receive antenna encounters about 10% of its initial amplitude of 5 V. Under these conditions the RF tag is resonation. The diode signal is pinged when the signal generator transmits. From the traces shown in Figure 4.11, we conclude that the CNT-diode is acting as an RFID with under damped current characteristics.

4.3 CNT SEM Imaging Analysis

This thesis introduced the ideas of wafer cleaning, masking, lithography, etching, developing, DC sputtering, annealing, CVD process (CNTs are formed during this stage), and diode fabrication in a ceramic package. Between these stages tests were performed to validate results. Two types of validations were examined in this thesis. The first type of validation was how clean the wafers were in repeated methanol and acetone baths with movement. The elimination of more photoresist on the samples had a better tendency to increase field emissions.The second type of validation was how long, how dense, and visual defects in CNTs

after the CVD process. A Scanning Electron Micrscope (SEM) was used to examine these processes and help validate conclusions. A JEOL or ZEISS SEM with the ability to analyze the light spectrum of the composition of the material and at least the ability to magnify normal definition 100,000 times. The SEM was able to verify the iron DC sputtering was 99.999% pure iron [33] and an overall composition of carbon and iron. This information also helps us verify metallic nanotubes.

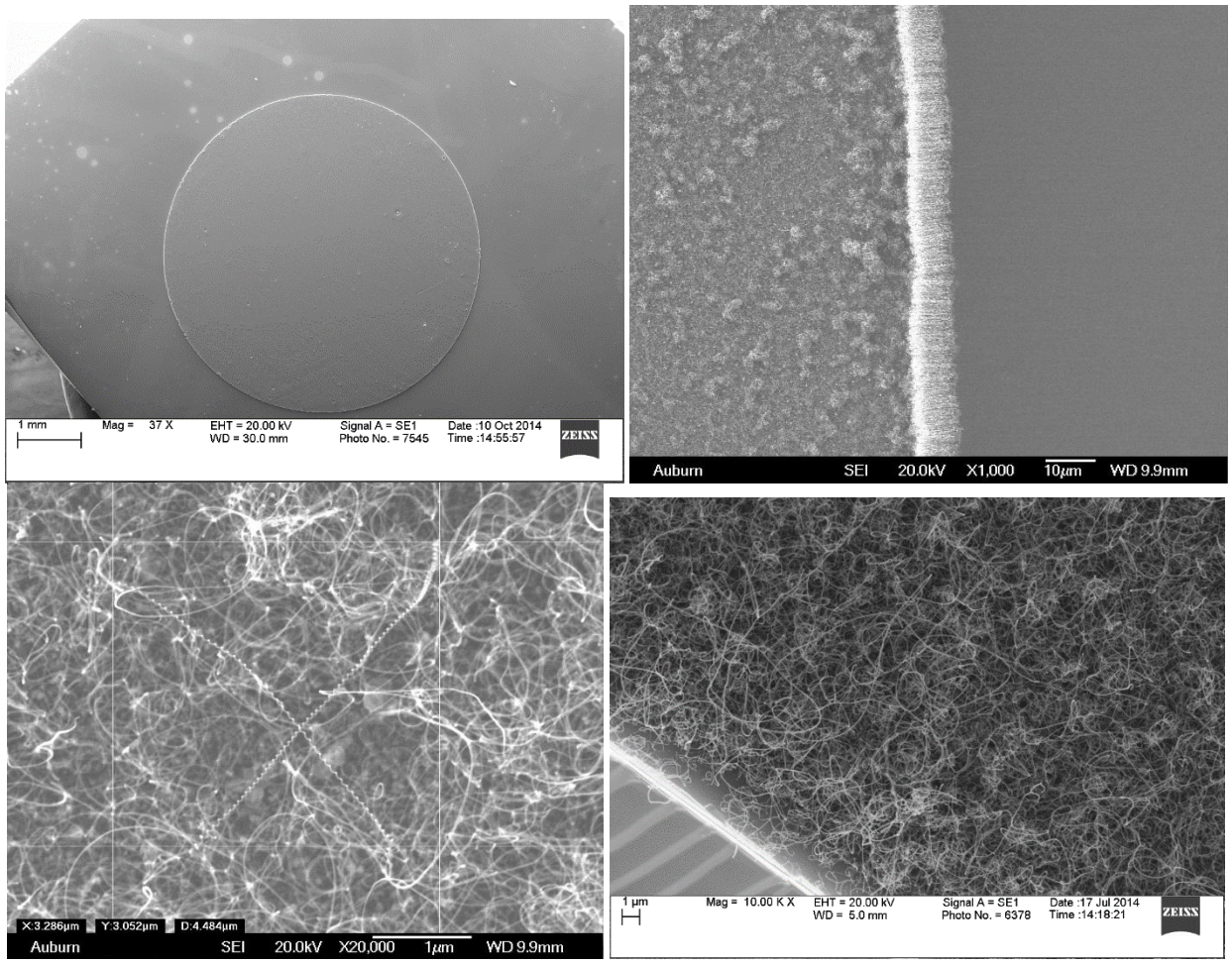

Figure 4.12 (Top Left) The circular shaped iron sputtered pattern after removing photoresist. (Top and Bottom Right) Side lips of the CNT shaped area with different magnifications. (Bottom Left) A measurement of a spiral CNT. The length and height are measured with the SEM. Length is measured to be approximately 4.4µm on each CNT strand (diagonal measurement shown).

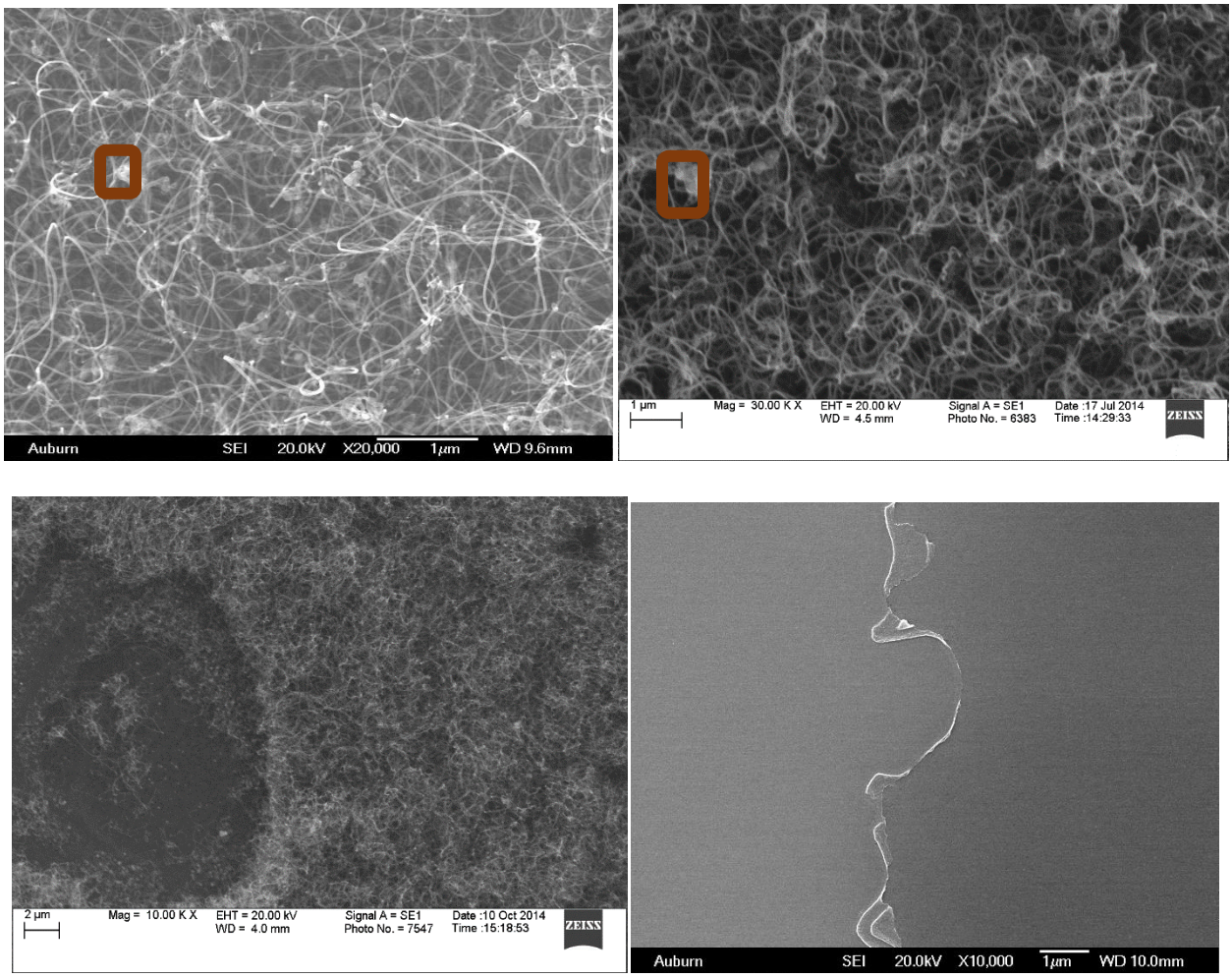

Figure 4.13 (Top) Nodules in the matrix of CNTs that are caused by impurities. (Bottom Left) A very sparse area of CNTs in a patterned sample. (Bottom right) Photoresist on an iron DC sputtered sample.

Impurities from carbon nanotubes can cause destructive unwanted characteristics or desirable characteristics tailored to particular functions [41]. An example are peapod carbon nanotubes [4] where fullerene balls are enclosed within the Carbon nanotubes. SEM can also identify structural destruction in the formation of CNTs. Sometimes the carbon nanotube will fail to bond to neighboring carbon atoms causing a tear in the tube [4].

Chapter 5
Results and Conclusions

A MWCNT vacuum diode was created in this thesis. A substrate was prepared, DC sputtered with iron, annealed and applied acetylene during CVD process at certain parameters of gas proportions, with transport gasses, pressures, vacuum, temperatures and distances. The patterned shape of CNT was chemically bonded to a ceramic package. Gold leads were attached to an anode and cathode and a vacuum in a nitrogen rich atmosphere encapsulated the CNTs. The diode's application was tested as a RFID tag. The current vacuum tube's turn on voltage is 1.5V/μm^2 which is lower than previous research studies. Field emissions and SEM images were examined on 42 samples as seen in the appendix of this thesis. A portion of the SEM images and data is shown in the appendix. The diode was integrated with wire recreating resistance, capacitance and inductance values at UHF frequencies. The passive, near field, RFID tag saw noise but had a clear resonance frequency of 300MHz by FFT measurement from an oscilloscope. In figure 42, another CNT diode thesis was prepared in a glass substrate with roughly the same turn on voltage.

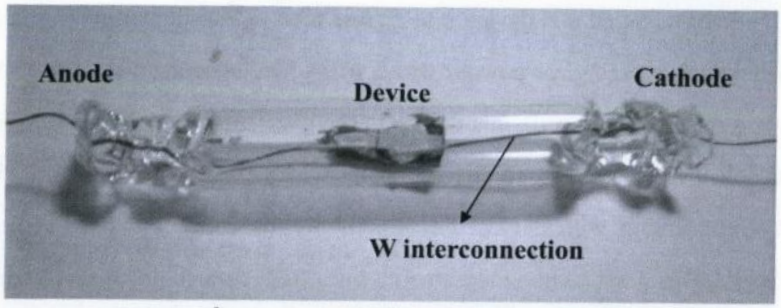

Fig. 4.29 The image of a fully packaged lateral carbon nanotubes field emission diode

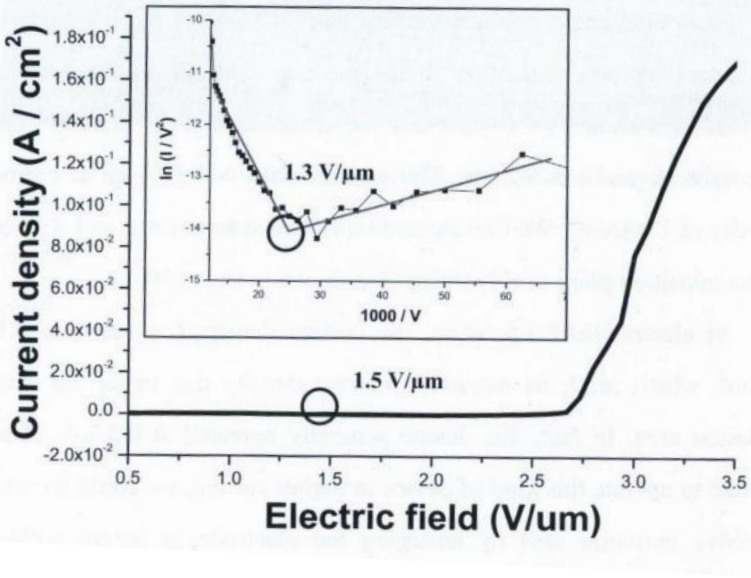

Figure 5.1 (top) a lateral carbon nanotube vacuum diode in glass. (bottom) field emission characteristics of vacuum diode. [42]

References

[1] Menzel, Donald H. *Fundamental formulas of physics*. New York: Dover, 1960. Print.

[2] L.M. Peng, Z. L. Zhang, Z. Q. Xue, Q. D. Wu, Z. N. Gu, and D. G. Pettifor, Phys. Rev. Lett.85, 3249 (2000).

[3] P.G. Collins & P. Avouris, Nanotubes for Electronics, Scientific American, 2000. Print.

[4] O'Connell, Michael. *Carbon nanotubes: properties and applications*. Boca Raton, FL: CRC/Taylor & Francis, 2006. Print.

[5] Bethune, D.S., Kiang, C.H., de Vries, M.S., Gorman, G., Savoy, R., Vazquez, J., and Beyers, R., "Cobalt-Catalyzed Growth of Carbon Nanotubes with Single-Atomic Layer Walls", *Nature* 363, 605-607, 1993.

[6] Harris, Peter J. *Carbon nanotube science : synthesis, properties and applications*. Cambridge, UK New York: Cambridge University Press, 2011. Print.

[7] Bandaru, Prabhakar R., "Electrical Properties and Applications of Carbon Nanotube Structures". *Journal of Nanoscience and Nanotechnology*. Vol.7, 1–29, 2007.

[8] T. Lin, B. Bajpai, T. Ji, L. Dai "Chemistry of Carbon Nanotubes". Csiro Publishing Aust. J. Chem. 2003, 56 , 635–651. 1 May 2003.

[9] Zhao Haitao, Kirkici Hulya. " Carbon Nanotube (CNT) Triggered Pseudospark Switch" Auburn University, 2012.

[10] Z. Wu, L. Wang, and H. Xin, "High Frequency Characterization of Carbon Nanotube Films," Accepted, 33rd International Conference on Infrared, Millimeter, and THz Waves, Sept. 2008.

[11] Reich, S, C Thomsen, and J Maultzsch. *Carbon nanotubes: basic concepts and physical properties*. Weinheim Cambridge: Wiley-VCH, 2004. Print.

[12] Dresselhaus, M. S., G Dresselhaus, and P. C. Eklund. *Science of fullerenes and carbon nanotubes*, San Diego: Academic Press, 1996. Print.

[13] Yakupoglu, Baha. *Synthesis of Carbon Nanotubes (CNTs) as Thermal Interface Material*. Thesis. Auburn University, 2013. Print.

[14] Zhang, Qing. *Carbon nanotubes and their applications*. Singapore: Pan Stanford Publishing, 2012. Print.

[15] Jaeger, Richard C. *Introduction to microelectronic fabrication*. Upper Saddle River, N.J: Prentice Hall, 2002. Print.

[16] H.Zhao, *Design and gConstruction of Carbon NanoTubes (CNTs) Triggered Pseudospark Switch,* Thesis. Auburn University, 2012. Print.

[17] Fan Shoushan, Liang Wenjie, Dang Haiyan, Franklin Nathan, Tombler Thomas, Chapline Michael, Dai Hongjie. "Carbon Nanotube Arrays on Silicon Substrates and their Possible Application" *Physica E*. volume 8, 180, 2000.

[18] Kloeffler, Royce Gerald *Electron Tubes*, Hoboken, New Jersey: John Wiley & Sons, INC, 1965. Print.

[19] ARRL, ed. *The Radio Amateur's Handbook*. West Hartford, Connecticut, U.S.A.:S.N, 1957. Print.

[20] Philco-Ford Corporation TechRep Division. *Vacuum Tube and Semiconductor Fundamentals*. Fort Washington, Pennsylvania 1960. Print.

[21] Kumar Abhishek, Dhawan Nikhil. "Embedding of Carbon Nanotubes on p-Type Silicon for Use in Solar Cells and PV Devices" *ASME Conference on Nanochannels, Microchannels and Minichannels. ICNMM2008-62183. Darmstadt, Germany June 23 2008.*

[22] Feynman, Richard P., Robert B. Leighton, and Matthew L. Sands. *The Feynman lectures on physics*. New York: Basic Books, a member of the Perseus Books Group, 2011. Print.

[23] Millikan, R. A. and Eyring, Carl F. (1926) *Laws Governing the Pulling of Electrons out of Metals by Intense Electrical Fields.* Physical Review, 27 (1). pp. 51-67. ISSN 0031-899X. *http://resolver.caltech.edu/CaltechAUTHORS:MILpr26d*

[24] Gomer, R. *Field emission and field ionization*. New York: American Institute of Physics, 1993. Print.

[25] Burkhardt, Charles E., and Jacob J. Leventhal. *Foundations of quantum physics*. New York: Springer, 2008. Print.

[26] Mott, Nevill F., and Howard Jones. *The theory of the properties of metals and alloys*. New York: Dover publ, 1958. Print.

[27] Léonard, François. *The physics of carbon nanotube devices*. Norwich, NY: William Andrew, 2009. Print.

[28] Burges R.E., Kroemer H., and Houston J.M.,. *Corrected Values of Fowler-Nordheim Field Emission Functions".* American Physical Society vol.90 No.4 1953. Print.

[29] Dyke W.P, and Dolan W.W., and Marton L., *Advances in Electrons and Electron Physics*, 8 Academic Press, New York 1956. Print

[30] Cheng, Yuan, and Zhou, Otto. “Electron Field Emission from Carbon Nanotubes”, *C.R Physique 4*, 1023-1033, 2003.

[31] Xiaowei, Sun. “Designing Efficient Field Emissio into ZnO”. *SPIE Newsroom*. DOI. 10.1117/2.1200602.0101 07 September 2006.

[32] Bai, Rujun. *Nonlinear Field Enhancement Factor of Carbon Nanotubes (CNTs) in Vacuum and Partial Pressure*. Thesis. Auburn University, 2013. Print.

[33] Tsai, Chung-Nan, and Kirkici, Hulya. “Field-Emission Characteristics of Selectively Grown CNTs”. *IEEE Transactions on Electron Devices*. Volume 60, Issue 1 Pages 478-481, 2013.

[34] Manohara Harish M., Bronikowski Michael J,. Hoenk Michael, Hunt Brian D., Siegel Peter H., “High-Current-Density Field Emitters Based on Arrays of Carbon Nanotube Bundles” *Jet Propulsion Laboratory, California Institute of Technology*. 29 September 2004.

[35] Dobkin, Daniel M. *The RF in RFID passive UHF RFID in practice*. Amsterdam Boston: Elsevier / Newnes, 2008. Print.

[36] Dorf, Richard C., and James A. Svoboda “Introduction to Electric Circuits” New York: John Wiley & Sons, 2004. Print.

[37] Finkenzeller, Klaus. *RFID handbook fundamentals and applications in contactless smart cards and identification*. Chichester, England Hoboken, N.J: Wiley, 2003. Print.

[38] Zhang Ming-Tao, Jiao Yong-Chang, Zhang Fu-Shun, Wang Wu-Tu. “Design of Antennas for RFID Application” *Development and Implementation of RFID Technology*. 554. February 2009.

[39] Ott, Henry W. *Noise reduction techniques in electronic systems*. New York: Wiley, 1976. Print.

[40] Betts, J.A., PHD. *High-frequency Communication*. London: Admiralty Signal Establishment, 1967. Print.

[41] Sohn, Jung Inn, Lee, Seonghoon, Song, Yoon-Ho, Choi, Sung-Yool , Cho, Kyoung-Ik , and Nam, Kee-Soo. "Patterned Selective Growth of Carbon Nanotubes and Large Field Emission from Vertically Well-Aligned Carbon Nanotube Field Emitter Arrays" *Applied Physics Letters.* Vol 78, Number 7. 12 February 2001.

[42] Yuan, Li. *Carbon Nanotubes Field Emission Diode Nanoelectronic Device*. Saarbrücken: VDM Verlag Dr. Müller, 2009. Print

Appendix

Sample CNT Result Report:

Date of Sputtering	Sputtering Conditions	CVD Conditions	Pattern	Other Steps	Other Observations
Sept. 24 , 2014 8 minutes FE	seconds watts Volts Amps 0 40 388 0.07 30 60 363 0.13 60 80 384 0.17 90 100 400 0.21	20 minutes 700°C Argon & Acetylene	circular	8 hours Annealing at 300°C	$ambient\ 3 * 10^{-6}\ torr$ Argon sputtering at 7mili-torr
Sept. 24 , 2014 8 minutes FE	Same sample as above	20 minutes 700°C Argon & Acetylene	circular	No	$ambient\ 3 * 10^{-6}\ torr$ Argon sputtering at 7mili-torr
Oct. 1 , 2014 5 minutes Fe	seconds watts Volts Amps 0 40 348 0.08 30 60 374 0.12 60 80 393 0.16 90 100 410 0.21	20 minutes 700°C Argon & Acetylene	circular	8 hours Annealing at 300°C	$ambient\ 4 * 10^{-6}\ torr$ Argon sputtering at 7mili-torr
Oct. 3 , 2014 3 minutes Fe	seconds watts Volts Amps 0 40 331 0.09 30 60 338 0.14 60 80 356 0.19 90 100 377 0.23	20 minutes 700°C Argon & Acetylene	circular	No	$ambient\ 3 * 10^{-6}\ torr$ Argon sputtering at 7mili-torr
Oct 4 , 2014 2 minutes Fe	seconds watts Volts Amps 0 40 400 0.06 30 60 373 0.12 60 80 398 0.17 90 100 412 0.21	20 minutes 700°C Argon & Acetylene	circular	No	$ambient\ 3 * 10^{-6}\ torr$ Argon sputtering at 7mili-torr
Oct. 5 , 2014 2 minutes Fe	seconds watts Volts Amps 0 40 346 0.08 30 60 374 0.12 60 80 393 0.17 90 100 404 0.21	CVD process after July 10th, 2014	circular	No	$ambient\ 3 * 10^{-6}\ torr$ Argon sputtering at 7mili-torr
Oct. 9 , 2014 3 minutes Fe	seconds watts Volts Amps 0 40 340 0.08 30 60 366 0.13 60 80 384 0.17 90 100 397 0.22	20 minutes 700°C Argon & Acetylene	circular	No	$ambient\ 3 * 10^{-6}\ torr$ Argon sputtering at 7mili-torr

Sept. 24th without annealing:

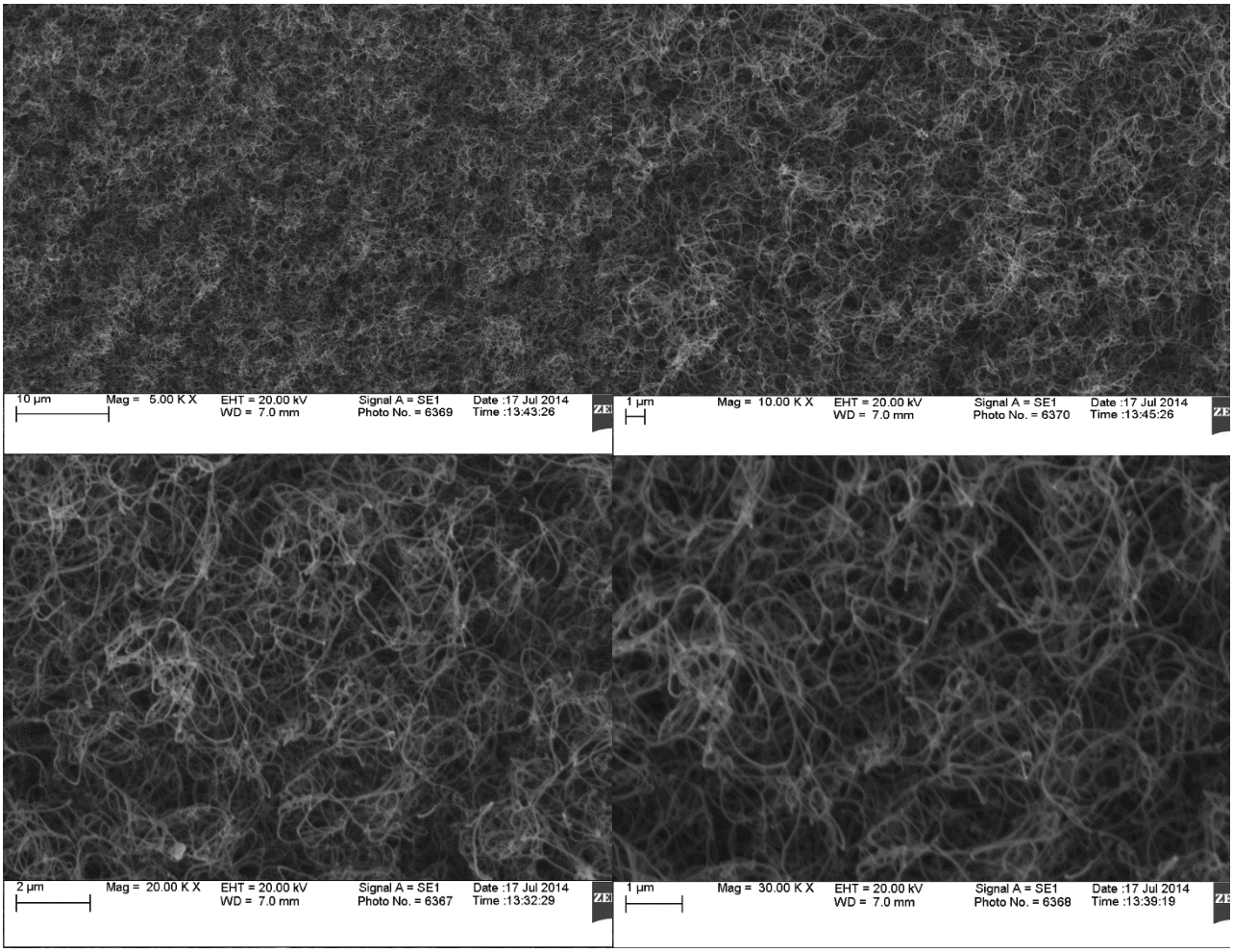

Sept. 24th with annealing:

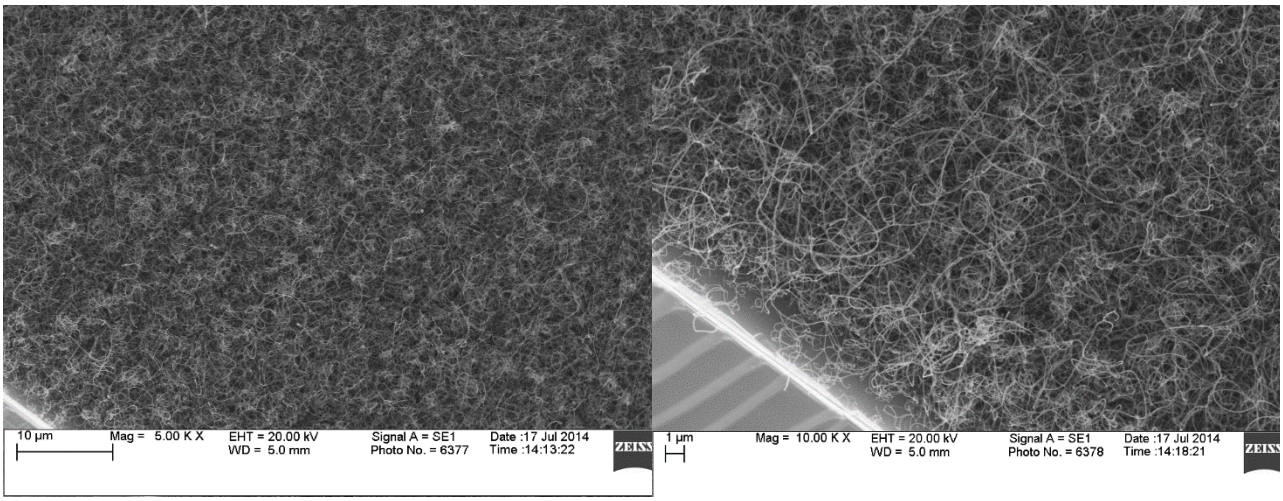

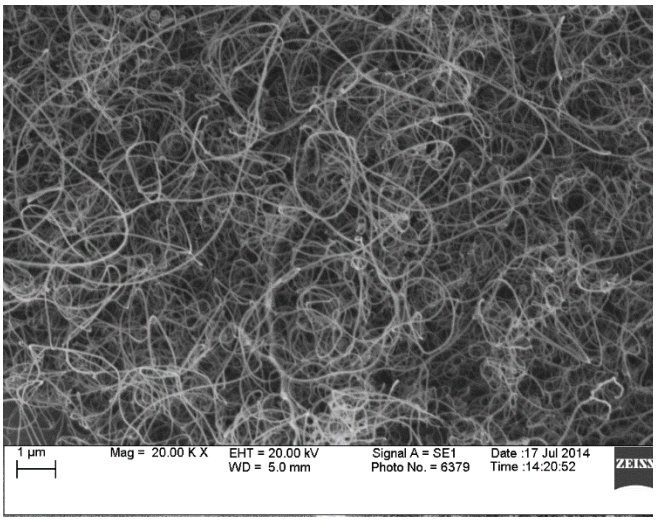
1 µm
Mag = 20.00 K X
EHT = 20.00 kV
WD = 5.0 mm
Signal A = SE1
Photo No. = 6379
Date :17 Jul 2014
Time :14:20:52

Oct. 1st:

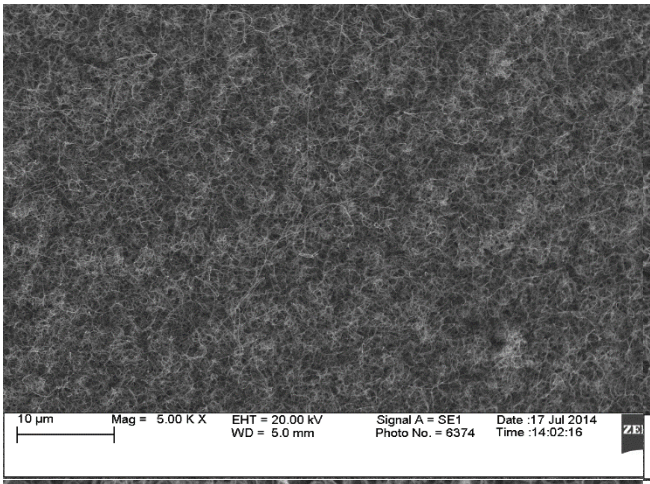
10 µm
Mag = 5.00 K X
EHT = 20.00 kV
WD = 5.0 mm
Signal A = SE1
Photo No. = 6374
Date :17 Jul 2014
Time :14:02:16

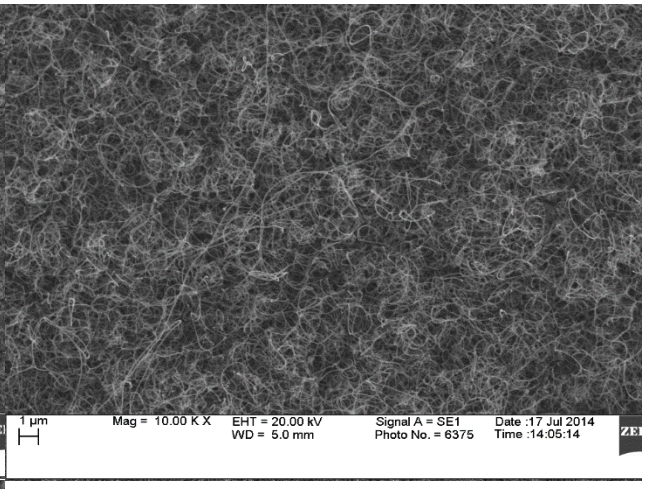
1 µm
Mag = 10.00 K X
EHT = 20.00 kV
WD = 5.0 mm
Signal A = SE1
Photo No. = 6375
Date :17 Jul 2014
Time :14:05:14

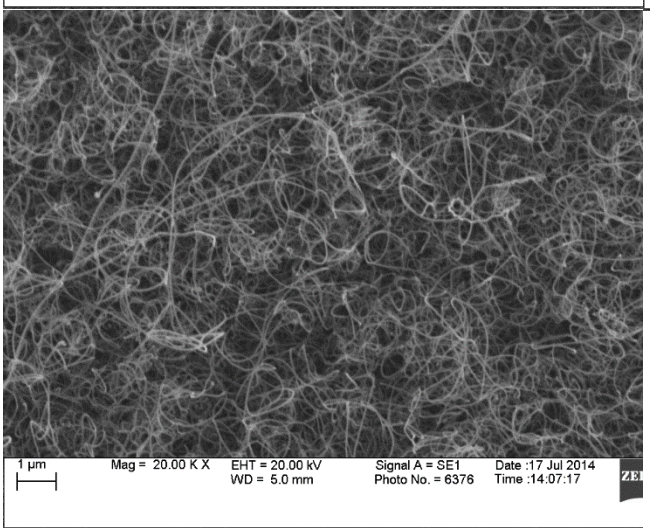
1 µm
Mag = 20.00 K X
EHT = 20.00 kV
WD = 5.0 mm
Signal A = SE1
Photo No. = 6376
Date :17 Jul 2014
Time :14:07:17

Oct. 3rd:

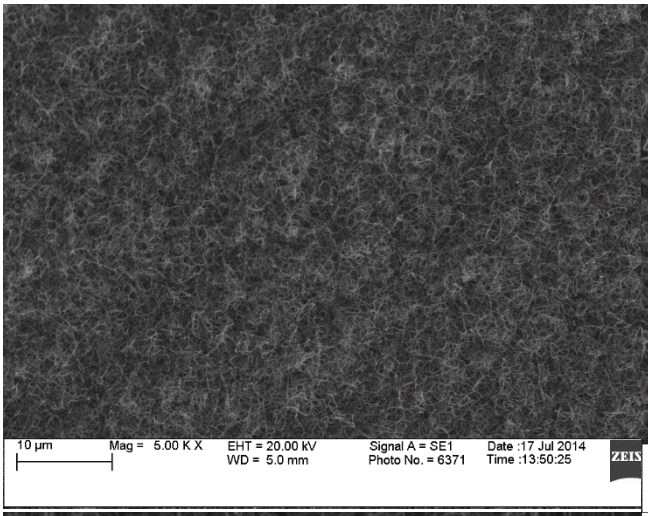

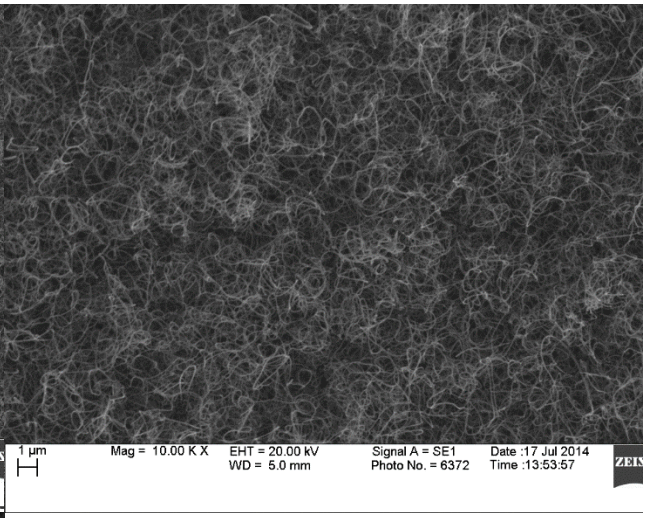

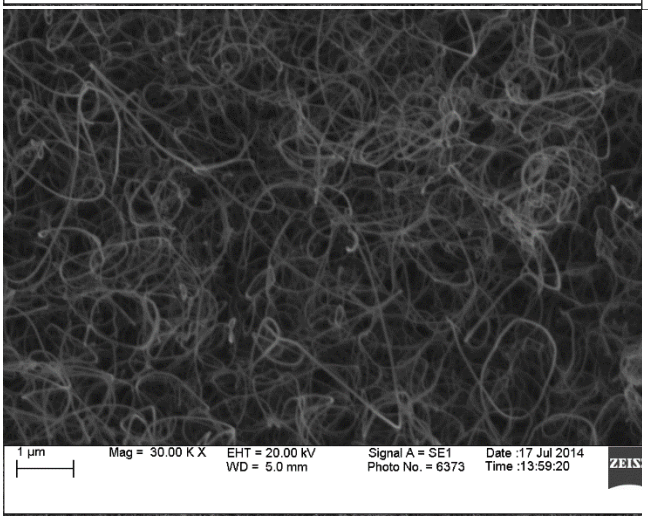

Oct 4th:

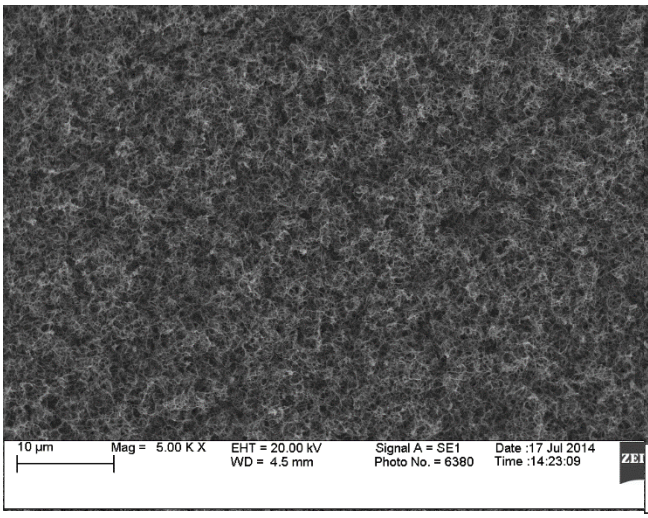

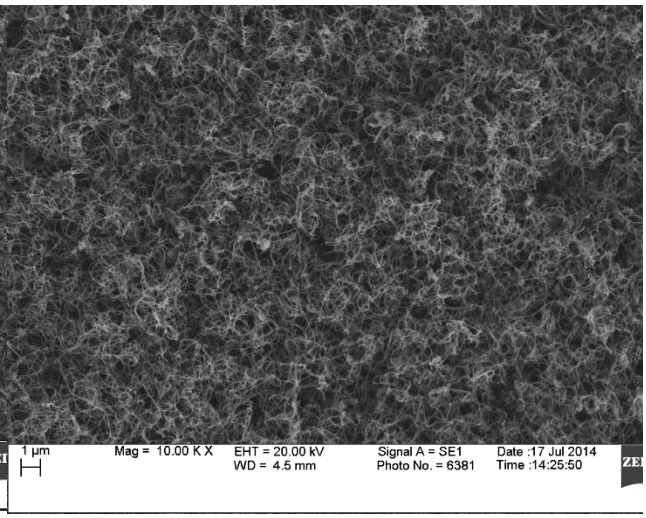

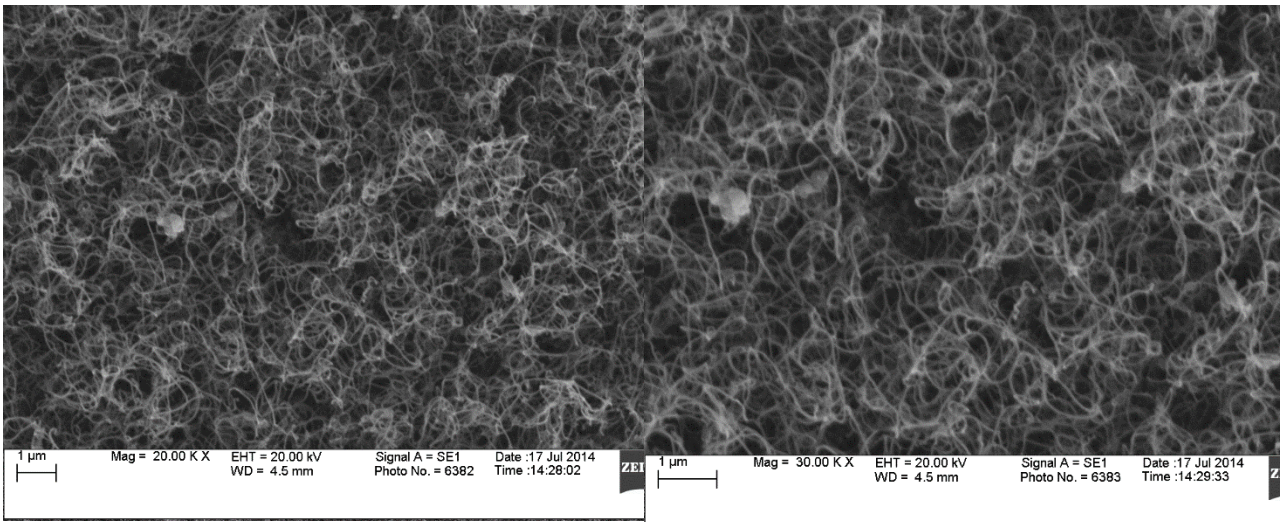

Sept. 24 without annealing:

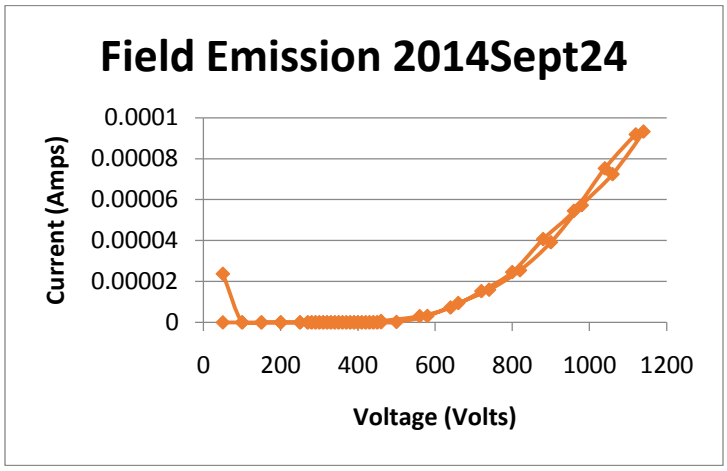

Sept. 24 with annealing:

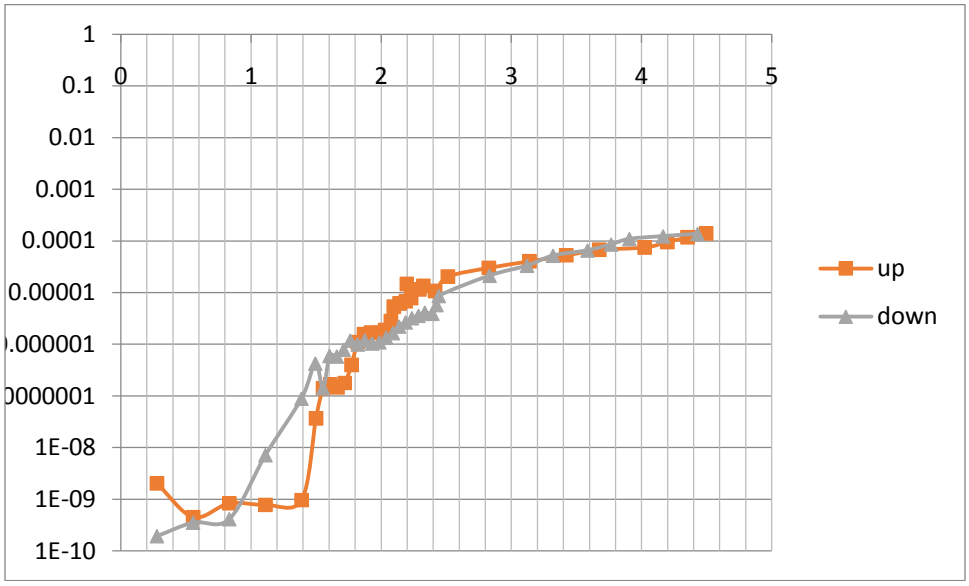

Oct. 1:

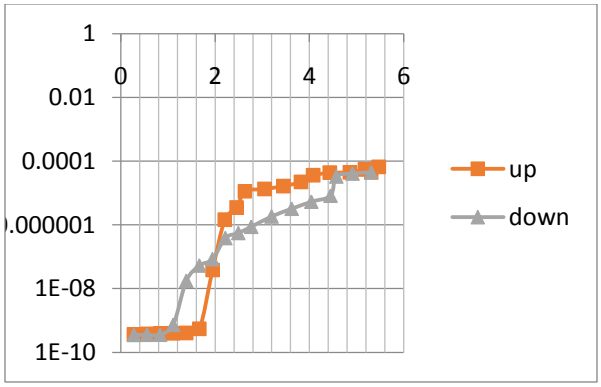

Oct. 3:

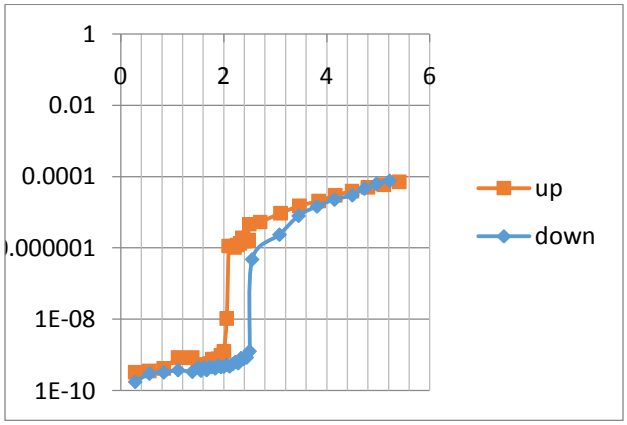

Oct. 4:

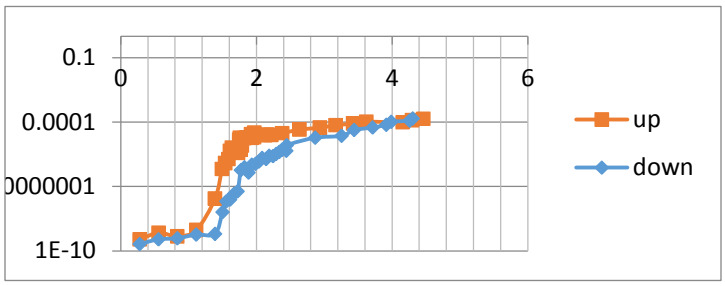

Full List of all premade samples*:

Batch	date	shape
1	Aug. 4, 2014	square
2	Aug. 8, 2014	square
3	Aug. 13, 2014	square
4	Aug. 15, 2014	square
5	Aug. 20, 2014	square
6	Aug. 21, 2014	Square
7	Aug. 25, 2014	square
8	Sept. 5, 2014	square
9	Sept. 7, 2014	square
10	Sept. 11, 2014	square
11	Sept. 17, 2014	square
12	Sept. 19, 2014	circle
13	Sept. 24, 2014	circle
14	Sept. 26, 2014	circle
15	Sept. 27, 2014	circle
16	Oct. 1, 2014	circle
17	Oct. 3, 2014	circle
18	Oct. 4, 2014	circle
19	Oct. 5, 2014	circle
20	Oct. 9, 2014	circle
21	Oct. 10, 2014	circle
22	Oct. 12, 2014	circle
23	Oct. 13, 2014	circle
24	Oct. 14, 2014	circle
25	Oct. 15, 2014	circle
26	Oct. 16, 2014	circle
27	Oct. 17, 2014	circle
28	Oct. 19, 2014	FULL
29	Oct. 24, 2014	circle
30	Oct. 27, 2014	circle
31	Oct. 29, 2014	circle
32	Oct. 31, 2014	circle
33	Nov. 2, 2014	circle
34	Nov. 6, 2014	circle
35	Nov. 16, 2014	circle
36	Nov. 20, 2014	circle
37	Nov. 23, 2014	circle
38	Dec. 2, 2014	circle
39	Dec. 3, 2014	circle
40	Dec. 4, 2014	circle
41	Dec. 7, 2014	circle
42	Dec. 14, 2014	circle

*All 42 samples had photos of final samples but cannot be stored onto this Thesis file.